Canadian Mineralogist
Vol. 29, pp. 909-942 (1991)

UNIFIED DESCRIPTION OF INCONGRUENT REACTIONS AND MINERAL SOLUBILITIES AS A FUNCTION OF BULK COMPOSITION AND SOLUTION pH IN HYDROTHERMAL SYSTEMS

VITALII A. POKROVSKII AND HAROLD C. HELGESON
Department of Geology and Geophysics, University of California, Berkeley, California 94720, U.S.A.

ABSTRACT

Depiction of mineral solubilities on isobaric isothermal bulk composition – pH diagrams facilitates considerably the correlation of the consequences of irreversible reactions with the solubilities of incongruent reaction products. The reaction-progress variable (ξ) is related to the bulk composition variable (η_c, which has units of moles (kg H_2O)$^{-1}$) by the stoichiometries of the irreversible reactions and the relative rates of reaction of the reactant minerals. To illustrate the advantages of using diagrams of this kind to describe simultaneously mineral solubilities, phase relations, and mass transfer resulting from reaction of minerals with hydrothermal fluids in both open and closed systems, equilibrium solubilities of stable minerals in the system K_2O–Na_2O–Al_2O_3–SiO_2–H_2O were computed as a function of pH in NaCl–HCl–NaOH–H_2O solutions in which m_{NaCl} = 0.01 or 1.0 at various pressures and temperatures of geological interest. These solubilities were then plotted together with representative reaction paths on $\eta_{Al_2Si_2O_5(OH)_4}$ – pH, $\eta_{KAl_3Si_3O_{10}(OH)_2}$ – pH, $\eta_{KAlSi_3O_8}$ – pH, and $\eta_{NaAlSi_3O_8}$ – pH diagrams. Consideration of these diagrams indicates that kaolinite, muscovite, and K-feldspar dissolve congruently only over relatively narrow ranges of solution pH. Above and below the pH limits of these ranges, the minerals dissolve incongruently to form quartz, diaspore, or aluminosilicates. Albite dissolves incongruently over the entire range of solution pH from zero to 12. Changes in solution composition and the identities and number of moles of minerals that precipitate and dissolve along incongruent reaction paths can be assessed directly from bulk composition – pH diagrams, which can also be used to interpret phase relations in terms of mineral solubilities over wide ranges of pressure, temperature, and fluid composition.

Keywords: mineral solubility, incongruent reaction, bulk composition, pH, kaolinite, muscovite, K-feldspar, albite.

SOMMAIRE

Une représentation de la solubilité des minéraux au moyen de diagrammes de composition *versus* pH, conçus pour pression et température constantes, facilite considérablement la corrélation des conséquences des réactions irréversibles avec la solubilité des produits des réactions incongruentes. La variable ξ qui marque le progrès d'une réaction est liée à la variable η_c, qui représente la composition globale par la stoechiométrie des réactions irréversibles et par le taux relatif d'une réaction impliquant les phases minérales réactives. Afin d'illustrer les avantages de tels diagrammes pour décrire simultanément les solubilités de phases minérales, les relations de phases, et le transfert de matière résultant de la réaction de minéraux avec une phase fluide hydrothermale dans un système ouvert ou fermé, la solubilité des minéraux stables à l'équilibre dans le système K_2O–Na_2O–Al_2O_3–SiO_2–H_2O a été calculée en fonction du pH d'une solution contenant NaCl–HCl–NaOH–H_2O dans laquelle m_{NaCl} est soit 0.01 ou 1.0, et ce, à plusieurs valeurs de pression et de température d'intérêt géologique. Ces solubilités sont ensuite presentées graphiquement avec des trajectoires de réaction typiques en termes de $\eta_{Al_2Si_2O_5(OH)_4}$ – pH, $\eta_{KAl_3Si_3O_{10}(OH)_2}$ – pH, $\eta_{KAlSi_3O_8}$ – pH, et $\eta_{NaAlSi_3O_8}$ – pH. A la lumière de ces diagrammes, kaolinite, muscovite et feldspath potassique entrent en solution de façon congruente seulement sur un intervalle restreint de pH de la solution. A un pH plus élevé ou plus faible, ces minéraux entrent en solution de façon incongruente pour former quartz, diaspore ou les aluminosilicates. Par contre, l'albite se dissout de façon incongruente pour tout pH compris entre 0 et 12. Il est ensuite possible d'évaluer les changements dans la composition d'une solution et dans l'identité et le nombre de moles de minéraux qui précipitent ou se dissolvent le long de la trajectoire d'une réaction incongruente d'après ces diagrammes de composition globale en fonction de pH. Ils servent aussi à interpréter les relations de phase en fonction de solubilités des phases minérales sur un grand intervalle de pression, température, et composition de la phase fluide.

(Traduit par la Rédaction)

Mots-clés: solubilité de phases minérales, réaction incongruente, composition globale, pH, kaolinite, muscovite, feldspath potassique, albite.

INTRODUCTION

Prediction of the equilibrium solubilities of rock-forming minerals in aqueous electrolyte solutions involved in geochemical processes provides a frame of reference for interpreting the composi-

tions of these fluids and the extent to which they react with their mineralogical environment. Many geochemical processes take place at constant temperature and pressure. Under these conditions, the solubilities of minerals are controlled primarily by the solution pH. The pH of natural aqueous solutions ranges from <1 in mine waters and areas of recent volcanic and geothermal activity to 12 in solutions involved in the weathering of ultramafic igneous rocks (Ellis & Mahon 1964, Ivanov 1975, Barnes & O'Neil 1969, Barnes 1985, Varekamp & Kreulen 1990, Nordstrom *et al.* 1991, and others). Comprehensive calculation of the extent to which mineral solubilities depend on pH is fundamental to our understanding of phase relations in hydrothermal systems. These solubilities can be portrayed on bulk composition – pH diagrams (Helgeson 1970b, Sokolova & Khodakovskiy 1977, Pokrovskii & Ivanov 1982, Nesbitt 1984, Pokrovskii 1989), which can then be used to assess the consequences of the chemical interaction of hydrothermal fluids with minerals in geochemical processes. The purpose of the present communication is to (1) formalize the relation between mineral solubilities and reaction paths on such diagrams, and (2) demonstrate with the aid of phase relations in the system K_2O–Al_2O_3–SiO_2–HCl–NaCl–NaOH–H_2O how they can be used to advantage in assessing mineral solubilities and predicting changes in fluid composition and the identities and relative amounts of products of incongruent reaction formed and destroyed during reaction of hydrothermal fluids with their mineralogical environment.

Reaction Progress and Mineral Solubility

To illustrate the relation of the concept of reaction progress to the solubilities of incongruent reaction products, let us consider a hypothetical system consisting of three thermodynamic components designated by A–B–H_2O, in which the components A and B form crystalline phases with the compositions A, B, and AB. Phase relations in this system are depicted schematically in Figure 1. Diagrams of the kind shown in this figure have been used extensively to describe phase relations among minerals and aqueous solutions (Ricci 1951, Petersen 1965, Garrels & Mackenzie 1971, Nesbitt 1978, Pokrovskii & Sorokin 1983, and others) ever since Roozeboom (1894) and later Van't Hoff (1905, 1909) and Jänecke (1906) pioneered their application to the study of phase relations in salt deposits.

The irreversible dissolution of $AB_{(c)}$ in water can be described in terms of

$$AB_{(c)} \rightarrow A_{(aq)} + B_{(aq)} \qquad (1)$$

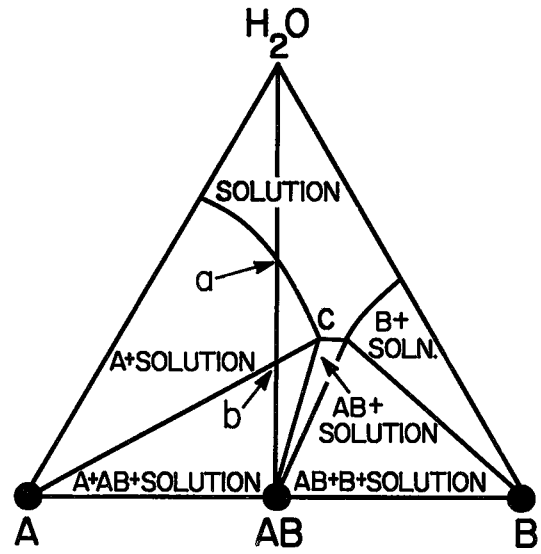

FIG. 1. Schematic phase diagram for the idealized hypothetical system A–B–H_2O at constant pressure and temperature (see text).

where the subscripts (*c*) and (*aq*) denote crystalline and aqueous states, respectively. Reaction (1) results initially in a change in solution composition from the H_2O apex in Figure 1 toward point *a*. This process can be described in terms of the reaction-progress variable (De Donder 1922, De Donder & Van Rysselberghe 1936, Helgeson 1968, 1970a, 1979) for reaction (1) by writing

$$\hat{n}_{AB_{(c)},(1)} \equiv \frac{dn_{AB_{(c)},(1)}}{d\xi_{(1)}} \qquad (2)$$

and

$$\xi_{(1)} = \frac{n_{AB_{(c)},(1)} - n^{\circ}_{AB_{(c)}}}{\hat{n}_{AB_{(c)},(1)}} \qquad (3)$$

where $n_{AB_{(c)},(1)}$ stands for the number of moles of $AB_{(c)}$ in the system after a given extent of reaction progress represented by the progress variable $\xi_{(1)}$, $n^{\circ}_{AB_{(c)}}$ refers to the number of moles of $AB_{(c)}$ in the system at $\xi_{(1)} = 0$, and $\hat{n}_{AB_{(c)},(1)}$ denotes the stoichiometric coefficient of $AB_{(c)}$ in reaction (1), which is equal to -1. As $\xi_{(1)}$ increases, the composition of the aqueous solution approaches saturation, with $A_{(c)}$ at point *a* in Figure 1. If the dissolution of $AB_{(c)}$ is the rate-limiting step in the process, further increase of $\xi_{(1)}$ along reaction path

ab is accompanied by formation of $A_{(c)}$ in accord with

$$A_{(aq)} \rightarrow A_{(c)} \tag{4}$$

as $\xi_{(1)}$ continues to increase and the composition of the solution changes along *ac*. At $\xi_{(1)}$ corresponding to point *b*, the composition of the solution reaches *c*, where it becomes saturated with $AB_{(c)}$ and overall equilibrium is achieved among $A_{(c)}$, $AB_{(c)}$, and the aqueous phase. However, in order for reaction (1) to achieve equilibrium, the bulk composition of the system must lie on the line connecting *b* and AB in Figure 1. For example, if instead the bulk composition coincides with a point on the line connecting *a* and *b* in Figure 1, all of the $AB_{(c)}$ in the system would have been consumed by the reaction, and the system would then consist simply of $A_{(c)}$ coexisting with the aqueous phase, which would have a composition at the right of point *a* and to the left of point *c* along the curve *ac*.

The relation between $\xi_{(1)}$ and the bulk composition of the system depicted in Figure 1 can be expressed in terms of the number of moles in the system of the compositional variable corresponding in stoichiometry to the mineral represented by $AB_{(c)}$ that have reacted (kg $H_2O)^{-1}$ (η_{AB}), which can be expressed as

$$\eta_{AB} \equiv \frac{n_{AB} - n_{AB_{(c)},(1)}}{W_{H_2O}} \tag{5}$$

where n_{AB} denotes the number of moles of AB in the system, and W_{H2O} designates the number of kilograms of H_2O in the aqueous phase, which is given by

$$W_{H_2O} \equiv n_{H_2O}\, M_w \tag{6}$$

where n_{H_2O} stands for the number of moles of H_2O in the aqueous solution, and M_w refers to the molecular weight of H_2O in kilograms. Combining Eqns. (3) and (5) leads to

$$\eta_{AB} \equiv \frac{n_{AB} - n^{\circ}_{AB_{(c)}} - \hat{n}_{AB_{(c)},(1)}\,\xi_{(1)}}{W_{H_2O}} \tag{7}$$

which couples reaction progress and bulk composition. For example, if the system depicted in Figure 1 is closed with respect to component AB (which is true for the reaction process described above), n_{AB} in Eqn. (7) is equal to $n^{\circ}_{AB(c)}$. Under these circumstances, Eqn. (7) reduces to

$$\xi_{(1)} = -\frac{W_{H_2O}\eta_{AB}}{\hat{n}_{AB_{(c)},(1)}} \tag{8}$$

where

$$\eta_{AB} \equiv \frac{n^{\circ}_{AB_{(c)}} - n_{AB_{(c)},(1)}}{W_{H_2O}} \tag{9}$$

In contrast, if the system is open to component AB and $n_{AB} \neq n^{\circ}_{AB(c)}$, it follows from Eqn. (7) that η_{AB} may continue to increase after equilibrium is reached if the bulk composition changes along *b*AB toward AB in Figure 1. Furthermore, in the absence of irreversible chemical reactions, $n_{AB_{(c)},(1)} = n^{\circ}_{AB(c)} = n^{\circ}_{AB}$, where n°_{AB} stands for the number of moles of AB in the system before any AB is added to, or removed from, the system. Under these circumstances, both Eqns. (5) and (7) can be written as

$$\eta_{AB} = \frac{n_{AB} - n^{\circ}_{AB}}{W_{H_2O}} \tag{10}$$

and for $n^{\circ}_{AB} = 0$,

$$\eta_{AB} = \frac{n_{AB}}{W_{H_2O}} \tag{11}$$

Equation (11) can be used to construct diagrams of mineral solubility in which one of the descriptive variables is η_{AB} by specifying a series of bulk compositions and minimizing the Gibbs free energy of the system for each one. In this way, mineral solubilities can be expressed in terms of η_{AB}, which can also be used to describe the consequences of irreversible reactions among minerals and the aqueous phase in the system.

Equation (7) can be generalized for any open or closed system by writing

$$\eta_c = \frac{n_c - n^{\circ}_c - \hat{n}_c\,\xi_{(1)}}{W_{H_2O}} \tag{12}$$

where η_c stands for the number of moles in the system of the compositional variable corresponding in stoichiometry to the mineral or mineral assemblage represented by the subscript *c* that have reacted or been added to, or removed from, the system (kg $H_2O)^{-1}$, n_c refers to the number of moles of the subscripted compositional variable in the system, n°_c denotes the number of moles of *c* in the system before any reactions have taken place or any *c* has been added to or removed from the system, ξ designates the overall progress variable for the reaction process (Helgeson 1970a, 1979), and $\hat{n}_c$ represents the overall stoichiometric reaction-coefficient defined by

$$\hat{n}_c \equiv \sum_{\phi} \sum_{r} \sigma_r \hat{n}_{\phi,r} \tag{13}$$

where $\hat{n}_{\phi,r}$ refers to the stoichiometric reaction-coefficient of the ϕth reactant mineral ($\phi = 1,2,\ldots, \hat{\phi}$) in the rth independent reaction ($r = 1,2,\ldots, \hat{r}$) representing irreversible dissolution of one mole of the subscripted mineral, and σ_r denotes the relative rate of reaction given by (Helgeson 1987)

$$\sigma_r \equiv \frac{d\xi_r}{d\xi} = \frac{d\xi_r / dt}{d\xi / dt} = \frac{d\xi_r / dt}{\sum_r d\xi_r / dt} \tag{14}$$

where ξ_r stands for the progress variable for the rth reaction, and t refers to time. It follows from these definitions that $d\xi / dt = \sum_r d\xi_r / dt$, $/\hat{\phi} = \hat{r}$, $\hat{n}_{\phi,r} = -1$, and $\hat{n}_c = -\sum_r$.

In many instances, $d\xi_r/dt$ in Eqn. (14) can be expressed as a function of the activity of the hydrogen ion. For example, if the subscript r refers to the hydrolysis of K-feldspar in acid solutions far from equilibrium, $d\xi_r / dt$ is given by (Helgeson *et al.* 1984)

$$\frac{d\xi_r}{dt} = \mathbf{k} s a_{H^+} \xi \tag{15}$$

where **k** stands for the rate constant, s refers to the effective surface area of the reactant feldspar, and a_{H^+} denotes the activity of the hydrogen ion.

If the general system considered above is closed to the compositional variable represented by the subscript c, it follows that $n_c = n_c^\circ$, and Eqn. (12) reduces to

$$\xi = -\frac{W_{H_2O} \eta_c}{\hat{n}_c} \tag{16}$$

where

$$\eta_c = \frac{n_{r,c}^\circ - n_{r,c}}{W_{H_2O}} = -\frac{\hat{n}_c \xi}{W_{H_2O}} \tag{17}$$

where $n_{r,c}^\circ$ and $n_{r,c}$ represent the total number of moles in the system of the reactant mineral or mineral assemblage represented by the subscript c at $\xi = 0$ and ξ, respectively, which are given by

$$n_{r,c}^\circ \equiv \sum_{\phi} \sum_{r} n_{\phi,r}^\circ \tag{18}$$

and

$$n_{r,c} \equiv \sum_{\phi} \sum_{r} n_{\phi,r} \tag{19}$$

where $n_{\phi,r}^\circ$ and $n_{\phi,r}$ denote the number of moles of the ϕth reactant mineral in the system prior to the rth reaction and the corresponding number of moles at any subsequent stage of reaction progress, respectively. It follows from these definitions that $\hat{n}_c$ in Eqn. (13) can also be expressed as

$$\hat{n}_c = \frac{dn_c}{\partial \xi} \tag{20}$$

The bulk composition of a system of $\hat{i}$ components can be expressed in terms of the mole fractions of the components, which are given by

$$X_i = \frac{n_i}{n} \tag{21}$$

where n_i and X_i stand for the number of moles and mole fraction of the ith thermodynamic component ($i = 1,2,\ldots,\hat{i}$) in the system, and

$$n \equiv \sum_{i} \left(n_{i,s} + \sum_{\phi} n_{i,\phi} n_{\phi} \right) \tag{22}$$

where $n_{i,\phi}$ refers to the number of moles of the ith component in the ϕth reactant mineral, and $n_{i,s}$ represents the number of moles of the ith component in the aqueous solution.

Although $\hat{n}_{\phi,r}$ in Eqn. (13) is a constant equal to -1, $\hat{n}_c$ is constant only if σ_r is independent of reaction progress for all values of r. Under these circumstances, $\hat{n}_c$ can be set to -1, and Eqn. (13) reduces to

$$\sum_r \sigma_r = 1 \tag{23}$$

If in addition the rates of all the irreversible dissolution reactions are equivalent,

$$\sigma_r = X_{\phi,r}^\circ = X_{\phi,r} \tag{24}$$

where

$$X_{\phi,r}^\circ = \frac{n_{\phi,r}^\circ}{n_c^\circ} \tag{25}$$

and

$$X_{\phi,r} = \frac{n_{\phi,r}}{n_c} \tag{26}$$

Although η_c is discussed above in the context of chemical reactions among minerals and an aqueous phase in systems closed to the compositional variable represented by the subscript c, it can also be used in the absence of irreversible reactions to describe the consequences of varying the bulk compositions of open systems. For example, in the absence of irreversible reactions, Eqn. (12) reduces to

$$\eta_c = \frac{n_c - n_c^\circ}{W_{H_2O}} \tag{27}$$

and for $n_c^\circ = 0$,

$$\eta_c = \frac{n_c}{W_{H_2O}} \tag{28}$$

If phase relations are depicted for any system on diagrams in terms of η_c and any other descriptive variable of interest, the diagrams can be used together with Eqn. (17) to describe the consequences of chemical reactions among minerals and aqueous solutions in either open or closed systems in terms of the solubilities of products of the incongruent reactions (see below). Expressing these solubilities as functions of η_c makes it possible to calculate the total molalities of the elements in the aqueous phase that correspond to those in the reactants from the stoichiometry of the compositional variable represented by c, which may correspond to that of a single mineral or an assemblage of minerals. In addition, it follows from Eqn. (16) that the number of moles of any given reaction product precipitated or dissolved along the reaction path can be computed from the difference between η_c and the value of η_c corresponding to the first appearance of the reaction product along the path. *Hence, the descriptive variable η_c serves a multiple purpose. It simultaneously represents 1) the equilibrium solubilities of minerals in units consistent with the molality scale of concentration, and 2) the consequences of the irreversible reaction of a mineral or mineral assemblage with the aqueous phase in terms of mineral solubilities and the overall progress variable for the process (kg H_2O)$^{-1}$.*

Combining the descriptive variable η_c with solution pH results in isothermal–isobaric η_c – pH diagrams that can be used to advantage in both interpreting the record of reaction paths preserved in metamorphic rocks and planning experimental investigations of metamorphic phase-relations in the laboratory. A number of diagrams of this kind are described below.

Isothermal–Isobaric η_c – pH Diagrams for the System K_2O–Al_2O_3–SiO_2–HCl–NaCl–NaOH–H_2O

Depending on the composition and pH of the aqueous phase, various charged and neutral aqueous species may contribute significantly to the solubilities of minerals in hydrothermal solutions. Of these, calculations based on thermodynamic analysis of experimental solubility data taken from sources cited in Table 1 indicate that the species shown in Table 2 predominate in aqueous electrolyte solutions coexisting with minerals in the system K_2O–Na_2O–Al_2O_3–SiO_2–H_2O at pressures and temperatures corresponding to those along the vapor–liquid equilibrium curve for the system H_2O. Thermodynamic calculations also indicate that the aqueous species listed in Table 2 account for the bulk of the solute in these solutions over the entire pH range from 1 to 12. The calculations were carried out using the revised HKF (Helgeson *et al.* 1981) equations of state (Tanger & Helgeson 1988, Shock & Helgeson 1988, 1990, Shock *et al.* 1989, 1992), together with the Hückel (1925) and Setchénow (1892) equations for the activity coefficients of aqueous species (Helgeson *et al.* 1981). Polynuclear complexes of aluminum and silicon form to appreciable degrees only in solutions that are highly supersaturated with respect to stable minerals, and the degrees of formation of mononuclear species such as $H_2SiO_4^{2-}$ and $HSiO_4^{3-}$ become appreciable only at values of solution pH greater than 12 at the pressures and temperatures considered in the present study (Baes & Mesmer 1976, Busey & Mesmer 1977). Accordingly, only the species shown in Table 2 were considered in the solubility calculations described below. The dielectric constant, density, and thermodynamic properties of H_2O used in the calculations were generated using equations and parameters taken from Johnson & Norton (1991). The apparent standard partial molal Gibbs free energies of formation of the aqueous species shown in Table 2 were calculated as a function of temperature and pressure with the aid of the revised HKF (Helgeson *et al.* 1981) equations of state (Tanger & Helgeson 1988, Shock & Helgeson 1988, Shock *et al.* 1989, 1992), summarized in Appendix A, using equations of state parameters and standard partial molal properties at 25°C and 1 bar taken from Tanger & Helgeson (1988), Shock & Helgeson (1988), Shock

TABLE 1. SUMMARY OF EXPERIMENTAL STUDIES OF THE EQUILIBRIUM SOLUBILITIES OF STABLE MINERALS REPORTED IN THE LITERATURE FOR THE SYSTEM K_2O–Na_2O–Al_2O_3–SiO_2–H_2O

Mineral or Mineral Assemblage	Temperature, Pressure	Initial Solution	Reference
Quartz	250–350°C, P_{SAT}	H_2O + NaOH	Tuttle & Friedman 1948
Quartz	250–450°C, 0.04–0.8 kbar	H_2O + NaOH	Friedman 1949
Quartz	160–373°C, P_{SAT}; 256–610°C, 0.15–1.75 kbar	H_2O	Kennedy 1950
Quartz	300–600°C, 0.2–2 kbar	H_2O	Morey & Hesselgesser 1951a
Quartz	300–500°C, 0.034–1.034 kbar	H_2O	Morey & Hesselgesser 1951b
Quartz	400°C, 0.24–2.5 kbar	H_2O + NaOH	Morey & Hesselgesser 1952
Quartz	200–355°C, 0.3 kbar	H_2O	Frederickson & Cox 1954
Quartz	400°C, 0.48 kbar; 410°C, 0.285 kbar; 470°C, 0.38 kbar	H_2O	Wyart & Sabatier 1954
Quartz	400°C, 0.5–2 kbar;	H_2O	Wyart & Sabatier 1955a
Quartz	500°C, 0.5 kbar	H_2O + NaCl, H_2O + NaOH, H_2O + KCl	Wyart & Sabatier 1955b
Quartz	400°C, 1.47–3.92 kbar	H_2O, H_2O + NaCl, H_2O + NaOH	Khitarov 1956
Quartz	200–600°C, 0.1–0.9 kbar	H_2O	Khitarov 1957
Quartz	500°C, 1 kbar	H_2O, H_2O + CO_2	Morey 1957
Quartz	300–400°C, 0.7–2.1 kbar	H_2O + NaOH	Laudise 1959
Quartz	60–100°C, P_{SAT}	H_2O, H_2O + NaCl, H_2O + NaOH, H_2O + $Na_2B_4O_7$	Van Lier *et al.* 1960
Quartz	140–370°C, P_{SAT}; 380–500°C, 0.49–0.91 kbar	H_2O	Kitahara 1960a
Quartz	140–420°C, 0.004–0.4 kbar	H_2O + NaCl	Kitahara 1960b
Quartz	400°C, 0.372 kbar	H_2O, H_2O + HCl, H_2O + NaOH	Kitahara 1960c
Quartz	300–400°C, 0.7–3.3 kbar	H_2O + NaOH	Laudise & Ballman 1961
Quartz	330°C, P_{SAT}	H_2O	Fyfe & McKay 1962
Quartz	25–240°C, P_{SAT}; 45–300°C, 1 kbar	H_2O	Morey *et al.* 1962
Quartz	125–181.5°C, P_{SAT}	H_2O, H_2O + KOH	Siever 1962
Quartz	400–550°C, 1–4 kbar	H_2O	Weill & Fyfe 1964
Quartz	400–500°C, 0.005–0.52 kbar	H_2O	Wendlandt & Glemser 1964
Quartz	500–900°C, 1–10 kbar	H_2O	Anderson & Burnham 1965
Quartz	100–250°C, 0.1–1.8 kbar;	H_2O + NaOH, H_2O + Na_2S	Learned 1966; Learned *et al.* 1967
Quartz	600–800°C, 3–4 kbar	H_2O, H_2O + NaCl, H_2O + KCl, H_2O + NaOH, H_2O + KOH	Anderson & Burnham 1967
Quartz	400–500°C, 1 kbar	H_2O + Ar	Sommerfeld 1967
Quartz	260°C, 0.06 kbar	H_2O + NaOH, H_2O + Na_2S	Ostapenko *et al.* 1969
Quartz	600–900°C, 0.7–3 kbar	H_2O	Semenova & Tsiklis 1970
Quartz	20°C, 1 bar	H_2O	MacKenzie & Gees 1971
Quartz	125–329°C, P_{SAT}	H_2O, H_2O + NaOH	Crerar & Anderson 1971
Quartz	285°C, 0.45 kbar	H_2O + HCl	Ostapenko & Arapova 1971a
Quartz	700°C, 5 kbar	H_2O, H_2O + CO_2	Shettel 1973
Quartz	500–900°C, 2–5 kbar	H_2O, H_2O + CO_2	Shettel 1974
Quartz	130–350°C, P_{SAT}	H_2O + $Na_2B_4O_7$, H_2O + $B(OH)_3$ + KOH	Seward 1974
Quartz	700°C, 3–5 kbar	H_2O + CO_2	Novgorodov 1975
Quartz	700°C, 1.5 kbar	H_2O, H_2O + NaCl, H_2O + CO_2	Novgorodov 1977
Quartz	200–350°C, P_{SAT}; 200–500°C, 1–2 kbar	H_2O, H_2O + NaCl, H_2O + KCl	Hemley *et al.* 1980
Quartz	350°C, 0.18–0.5 kbar	H_2O + NaCl	Fournier *et al.* 1982
Quartz	250°C, 0.25–1 kbar	H_2O	Ragnarsdóttir & Walther 1983
Quartz	350–550°C, 1–2 kbar; 600°C, 2 kbar; 400–618°C, 1–2 kbar	H_2O H_2O + CO_2 H_2O + Ar	Walther & Orville 1983
Quartz	400–450°C, 1 kbar	H_2O + NaOH	Sinitsyn & Ivanov 1984
Quartz	50–96°C, P_{SAT}	H_2O	Rimstidt 1984
Quartz	600°C, 2 kbar	H_2O + KOH	Pascal 1984
Quartz	300–475°C, 1 kbar	H_2O + NaOH	Sinitsyn 1986
Quartz	90°C, 1 bar	H_2O + NaOH	Schwartzentruber *et al.* 1987
Quartz	300°C, 1 kbar	H_2O + NaCl + $AlCl_3$ + HCl	Red'kin & Chevychelova 1988
Quartz	600–700°C, 2 kbar	H_2O + KOH	Pascal & Anderson 1989
Quartz	300–400°C, 0.5 kbar	H_2O + NaCl + $MgCl_2$	Saccocia & Seyfried 1990

TABLE 1 (CONTINUED)

Mineral or Mineral Assemblage	Temperature, Pressure	Initial Solution	Reference
Quartz	296°C, 1 kbar	H_2O, H_2O + HCl	Red'kin & Chevychelova 1991
Diaspore	200°C, P_{SAT}	H_2O + NaOH	Druzhinina 1955
Diaspore	250–300°C, P_{SAT}	H_2O + NaOH	Bernshtein & Matsenok 1965
Diaspore, Diaspore + Corundum	250–350°C, P_{SAT}	H_2O + NaOH	Wefers 1967
Diaspore	25°C, 1 bar	H_2O	Reesman & Keller 1968
Diaspore	250–325°C, P_{SAT}	H_2O + NaOH	Chang *et al.* 1979
Diaspore	25°C, 1 bar	H_2O + HCl	Peryea & Kittrick 1988
Diaspore	300°C, 1 kbar	H_2O + NaCl + $AlCl_3$ + HCl	Red'kin & Chevychelova 1988
Diaspore	25–350°C, P_{SAT}	H_2O + NaCl, H_2O + NaOH, H_2O + NaCl + NaOH	Apps *et al.* 1989
Diaspore	296°C, 1 kbar	H_2O, H_2O + HCl	Red'kin & Chevychelova 1991
Corundum	500°C, 1.034 kbar	H_2O	Morey 1957
Corundum	380–420°C, 0.25–0.49 kbar	H_2O, H_2O + NaOH	Yalman *et al.* 1960
Corundum	400–450°C, 0.51–1.52 kbar	H_2O + NaOH	Yamaguchi *et al.* 1962
Corundum	400–600°C, 0.31–2.8 kbar	H_2O + NaOH, H_2O + KOH, H_2O + NaCl, H_2O + KCl, H_2O + HCl	Barns *et al.* 1963
Corundum	328–515°C, 0.34–1.93 kbar	H_2O + $Na_2B_4O_7$	Levinson *et al.* 1965
Corundum	700–900°C, 2–6.75 kbar	H_2O, H_2O + NaCl, H_2O + KCl, H_2O + NaOH, H_2O + KOH	Anderson *et al.* 1987
Corundum	285°C, 0.45 kbar	H_2O + HCl	Ostapenko & Arapova 1971a
Corundum	500–800°C, 6 kbar	H_2O	Burnham *et al.* 1973
Corundum	350–500°C, 0.2–1.96 kbar	H_2O	Ganeev & Rumyantsev 1974
Corundum	670–700°C, 2.5– 6 kbar	H_2O	Becker *et al.* 1983
Corundum	400–700°C, 1–3 kbar	H_2O	Ragnarsdóttir & Walther 1985
Corundum	450–700°C, 1–2 kbar	H_2O + HCl, H_2O + NaCl, H_2O + KCl, H_2O + $AlCl_3$	Korzhinskiy 1987
Corundum	600°C, 2 kbar	H_2O + HCl	Baumgartner & Eugster 1988
Corundum	25°C, 1 bar	H_2O + HCl	Peryea & Kittrick 1988
Corundum	600°C, 2 kbar	H_2O + NaCl, H_2O + KCl	Pascal *et al.* 1989
Kaolinite	25°C, 1 bar	H_2O + HCl	Polzer & Hem 1965
Kaolinite	25°C, 1 bar	H_2O + HCl	Kittrick 1966
Kaolinite, Dickite, Pyrophyllite	25°C, 1 bar	H_2O	Reesman & Keller 1968
Andalusite, Kyanite	400–550°C, 1–3 kbar	H_2O	Brown & Fyfe 1971
Kyanite	285°C, 0.45 kbar	H_2O + HCl	Ostapenko & Arapova 1971a
Kyanite, Andalusite	420–500°C, 1.3 kbar	H_2O	Ostapenko & Arapova 1971b
Kaolinite	25°C, 1 bar	H_2O	Huang & Keller 1973
Pyrophyllite + Kaolinite	200–325°C, 1–2 kbar	H_2O	Hemley *et al.* 1980
Kaolinite + Diaspore	200–300°C, 1–2 kbar	H_2O	Hemley *et al.* 1980
Pyrophyllite + Diaspore	300–325°C, 1–2 kbar	H_2O	Hemley *et al.* 1980
Andalusite + Pyrophyllite	340–450°C, 1–2 kbar	H_2O	Hemley *et al.* 1980
Andalusite + Diaspore	350–390°C, 1 kbar	H_2O	Hemley *et al.* 1980
Andalusite + Corundum	400–500°C, 1–2 kbar	H_2O	Hemley *et al.* 1980
Kaolinite + Quartz	150–290°C, 0.98 kbar	H_2O + $AlCl_3$ + HCl	Red'kin & Ivanov 1980
Pyrophyllite + Quartz	300–400°C, 0.98 kbar	H_2O + $AlCl_3$ + HCl	Red'kin & Ivanov 1980
Andalusite + Quartz	430–500°C, 0.98 kbar	H_2O + $AlCl_3$ + HCl	Red'kin & Ivanov 1980
Kaolinite	25°C, 1 bar	H_2O + HCl	Kittrick 1980
Kyanite	400–500°C, 1.3 kbar	H_2O + HCl	Ostapenko *et al.* 1987
Kaolinite + Diaspore	300°C, 1 kbar	H_2O + NaCl + $AlCl_3$ + HCl	Red'kin & Chevychelova 1988
Kaolinite	80°C, 1 bar	H_2O + HCl	Nagy & Lasaga 1990
Kaolinite + Diaspore	250–300°C, 1 kbar	H_2O, H_2O + HCl	Red'kin & Chevychelova 1991

TABLE 1 (CONTINUED)

Mineral or Mineral Assemblage	Temperature, Pressure	Initial Solution	Reference
Kaolinite + Quartz	250°C, 1 kbar	H_2O, H_2O + HCl	Red'kin & Chevychelova 1991
Kaolinite + Pyrophyllite	250–280°C, 1 kbar	H_2O, H_2O + HCl	Red'kin & Chevychelova 1991
Pyrophyllite + Diaspore	254–375°C, 1 kbar	H_2O, H_2O + HCl	Red'kin & Chevychelova 1991
Pyrophyllite + Andalusite	336–402°C, 1 kbar	H_2O, H_2O + HCl	Red'kin & Chevychelova 1991
Andalusite + Diaspore	336–433°C, 1 kbar	H_2O, H_2O + HCl	Red'kin & Chevychelova 1991
Andalusite + Corundum	372–433°C, 1 kbar	H_2O, H_2O + HCl	Red'kin & Chevychelova 1991
Andalusite + Quartz	402°C, 1 kbar	H_2O, H_2O + HCl	Red'kin & Chevychelova 1991
Albite	500°C, 0.4–2 kbar	H_2O	Morey & Hesselgesser 1951a
K–feldspar	500°C, 1–2 kbar	H_2O	Morey & Hesselgesser 1951a
K–feldspar, Albite	100–350°C, 0.003–0.34 kbar	H_2O	Morey & Chen 1955
K–feldspar, Albite	500°C, 1 kbar	H_2O	Morey 1957
Muscovite	200–600°C, 0.3 kbar	H_2O	Khitarov 1957
K–feldspar + Muscovite + Quartz	200–500°C, 0.34–2.4 kbar 550–580°C, 1 kbar	H_2O + KCl + HCl	Hemley 1959; Hemley & Jones 1964; Montoya & Hemley 1975
Muscovite + Kaolinite	200–300°C, 0.14–2.4 kbar	H_2O + KCl + HCl	Hemley 1959; Hemley & Jones 1964
Muscovite + Pyrophyllite + Boehmite	300–450°C, 0.34–2.4 kbar	H_2O + KCl + HCl	Hemley 1959
Muscovite + Andalusite + Quartz	400–580°C, 1 kbar		Hemley 1959; Hemley & Jones 1964; Montoya & Hemley 1975
Albite + Paragonite + Quartz	300–500°C, 1.03 kbar	H_2O + NaCl + HCl	Hemley *et al.* 1961; Hemley & Jones 1964; Montoya & Hemley 1975
Paragonite + Pyrophyllite + Quartz	350–500°C, 1.03 kbar	H_2O + NaCl + HCl	Hemley *et al.* 1961; Hemley & Jones 1964
K–feldspar, Albite, Nepheline	295°C, 0.17 kbar	H_2O	Morey & Fournier 1961
Albite, Albite + Quartz	330°C, P_{SAT}	H_2O	Fyfe & McKay 1962
K–feldspar, K–feldspar + Quartz	300–600°C, 0.2–2.5 kbar	H_2O	Schloemer 1962
Muscovite, K–feldspar, Nepheline	25°C, 1 bar	H_2O	Reesman & Keller 1965
Albite	700°C, 2 kbar	H_2O	Adams 1968
Albite	400–600°C, 0.75–3.5 kbar	H_2O	Currie 1968
Muscovite	25°C, 1 bar	H_2O	Reesman & Keller 1968
Albite + Muscovite + Quartz, Albite + Paragonite, Paragonite + Pyrophyllite	450°C, 1 kbar	H_2O + NaCl	Althaus & Johannes 1969
Muscovite	100–350°C, P_{SAT}; 400–600°C, 0.3–3.1 kbar	H_2O	Strübel 1971
Albite	500–700°C, 2–8.4 kbar	H_2O	Davis 1972
K–feldspar, Muscovite	25°C, 1 bar	H_2O	Huang & Keller 1972
K–feldspar + Muscovite + Quartz	30–300°C, P_{SAT}	H_2O + KCl	Usdowski & Barnes 1972
Albite	25°C, 1 bar	H_2O	Huang & Keller 1973
K–feldspar + Muscovite + Quartz	400–700°C, 1–7 kbar	H_2O + KCl + HCl	Shade 1974
K–feldspar + Andalusite + Quartz	650–700°C, 1–7 kbar	H_2O + KCl + HCl	Shade 1974
Muscovite + Andalusite + Quartz	600–700°C, 1–7 kbar	H_2O + KCl + HCl	Shade 1974

TABLE 1 (CONTINUED)

Mineral or Mineral Assemblage	Temperature, Pressure	Initial Solution	Reference
Paragonite + Andalusite + Quartz	400–500°C, 1 kbar	H_2O + NaCl + HCl	Montoya & Hemley 1975
K–feldspar + Muscovite + Quartz	300–500°C, 0.98 kbar	H_2O + KCl + HCl	Ivanov *et al.* 1979
K–feldspar + Albite + Muscovite + Quartz	200–500°C, 0.98 kbar	H_2O + NaCl + KCl + HCl	Ivanov *et al.* 1979
K–feldspar + Muscovite + Quartz	600–670°C, 1–2 kbar	H_2O + KCl + HCl	Gunter & Eugster 1980
K–feldspar + Muscovite + Quartz	189–623°C, 2 kbar; 205°C, P_{SAT}	H_2O + KCl	Wintsch *et al.* 1980
Albite + Andalusite + Quartz	500–700°C, 1 kbar	H_2O + NaCl + HCl	Popp & Frantz 1980
K–feldspar + Leucite, Nepheline	500–600°C, 1–2 kbar	H_2O	Adcock & Mackenzie 1981
Albite + Muscovite + Quartz	300–500°C, 1 kbar	H_2O + NaCl + KCl + HCl	Pokrovskii 1982
Albite	125–350°C, P_{SAT}	H_2O + NaCl	Apps & Neil 1983
Muscovite	300°C, P_{SAT}	H_2O + NaOH	Mukhamet-Galeyev *et al.* 1984
Muscovite + Andalusite + Quartz	500–600°C, 2 kbar	H_2O + KCl + HCl	Pascal 1984; Anderson *et al.* 1987
Muscovite + Andalusite + Corundum	700°C, 2 kbar	H_2O + KCl + HCl	Pascal 1984; Anderson *et al.* 1987
K–feldspar + Andalusite + Quartz	700°C, 2 kbar	H_2O, H_2O + KCl + HCl	Pascal 1984; Anderson *et al.* 1987
K–feldspar + Muscovite + Andalusite	650°C, 2 kbar	H_2O	Pascal 1984; Anderson *et al.* 1987
K–feldspar + Andalusite + Corundum	700°C, 2 kbar	H_2O	Pascal 1984; Anderson *et al.* 1987
K–feldspar + Leucite + Muscovite	500°C, 2 kbar	H_2O	Pascal 1984; Anderson *et al.* 1987
K–feldspar + Leucite + Corundum	700°C, 2 kbar	H_2O	Pascal 1984; Anderson *et al.* 1987
Muscovite + Leucite + Corundum	500–600°C, 2 kbar	H_2O, H_2O + CO_2, H_2O + KCl	Pascal 1984; Anderson *et al.* 1987
K–feldspar + Muscovite + Quartz	500–700°C, 2.–2.38 kbar	H_2O, H_2O + KCl + HCl, H_2O + CO_2	Pascal 1984; Anderson *et al.* 1987
Albite + K–feldspar + Muscovite + Quartz	600°C, 2 kbar	H_2O + NaCl	Anderson *et al.* 1987
Albite + Paragonite + Quartz	350–500°C, 1–2.5 kbar	H_2O	Woodland & Walther 1987
K–feldspar + Muscovite + Quartz	300–550°C, 0.5–2 kbar	H_2O + KCl + HCl	Sverjensky *et al.* 1991
Muscovite + Andalusite + Quartz	400–550°C, 1–2 kbar	H_2O + KCl + HCl	Sverjensky *et al.* 1991
Muscovite + Pyrophyllite + Quartz	300–350°C, 1 kbar	H_2O + KCl + HCl	Sverjensky *et al.* 1991
Muscovite + Kaolinite + Quartz	300°C, 1 kbar	H_2O + KCl + HCl	Sverjensky *et al.* 1991
K–feldspar + Andalusite + Quartz	600°C, 1–2 kbar	H_2O + KCl + HCl	Sverjensky *et al.* 1991
Albite + Paragonite + Quartz	590°C, 3–6 kbar	H_2O + NaCl + HCl	Volfinger & Roux 1991

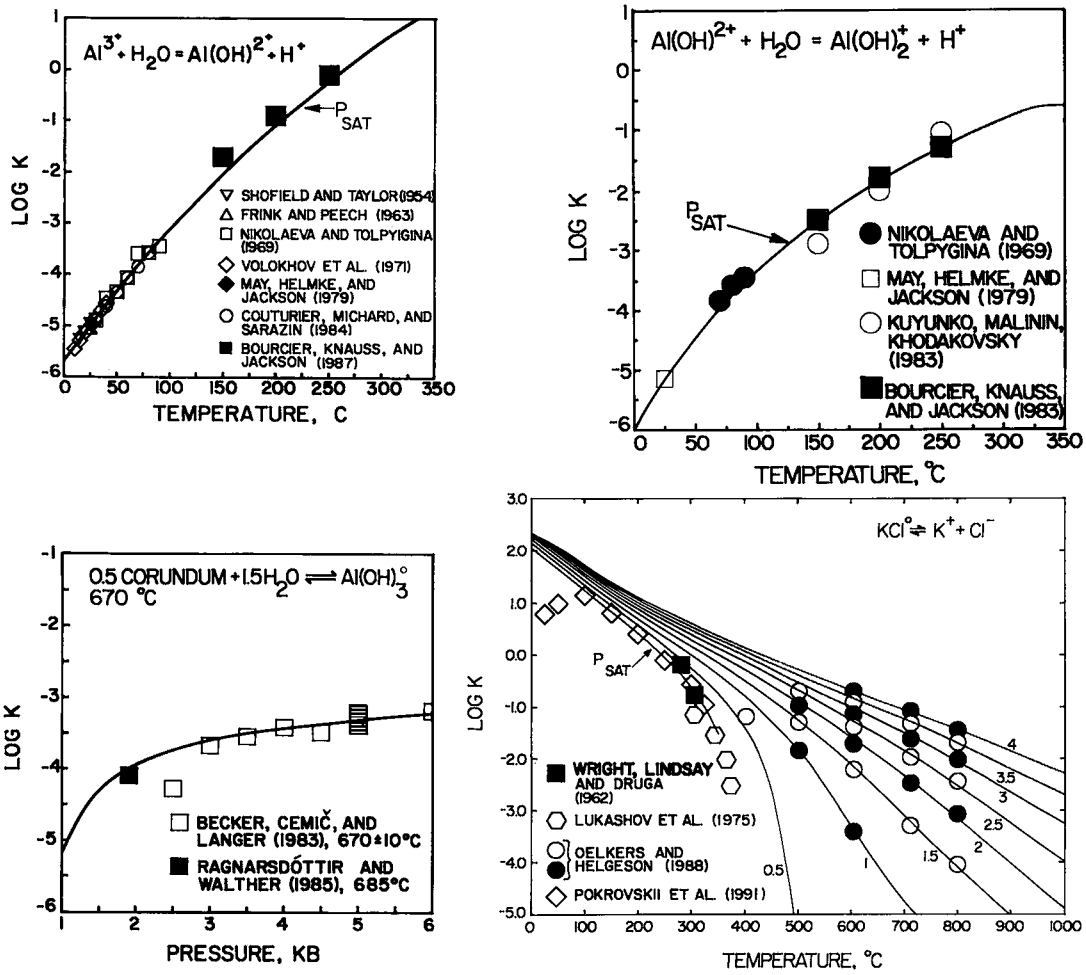

FIG. 2. Logarithm of equilibrium constants for hydrothermal reactions as a function of temperature at constant pressure (labeled in kilobars) or P_{SAT} or pressure at constant temperature (labeled in °C). The symbols represent experimental data taken from the literature, but the curves were generated by regression of the data using equations given in Appendix A, together with equations of state parameters and values of the thermodynamic properties of the aqueous species at 25°C and 1 bar taken from Pokrovskii & Helgeson (1989) and Pokrovskii *et al.* (1991).

TABLE 2. AQUEOUS SPECIES CONSIDERED IN THE PRESENT STUDY AND THE SOURCES OF THERMODYNAMIC DATA AND EQUATIONS OF STATE PARAMETERS USED TO CALCULATE THEIR RELATIVE STABILITIES AT ELEVATED TEMPERATURES AND PRESSURES

Species	Source of Thermodynamic Data and Equations of State Parameters
H^+, OH^-, Na^+, K^+, Cl^-	1
$NaCl^\circ$	2
KCl°, HCl°	3
SiO_2°	4
$H_3SiO_4^-$, $NaH_3SiO_4^\circ$, $KH_3SiO_4^\circ$	5
Al^{3+}, $Al(OH)^{2+}$, $Al(OH)_2^+$, $Al(OH)_3^\circ$, $Al(OH)_4^-$, $NaAl(OH)_4^\circ$, $KAl(OH)_4^\circ$, $NaOH^\circ$, KOH°	6

[1]Tanger & Helgeson (1988). [2]Shock *et al.* (1992). [3]Pokrovskii *et al.* (1991). [4]Shock *et al.* (1989). [5]V. A. Pokrovskii & H. C. Helgeson (in preparation). [6]Pokrovskii & Helgeson (1989).

et al. (1989, 1992), Pokrovskii & Helgeson (1989), Pokrovskii *et al.* (1991), and V.A. Pokrovskii & H.C. Helgeson (in prep.). Calculations of this kind were used together with Eqn. (A10) in Appendix A to generate the curves depicted in Figure 2. It can be seen in this figure that all of the curves representing the logarithms of the equilibrium constants for the reactions shown in the figure are in close agreement with their experimental counter-

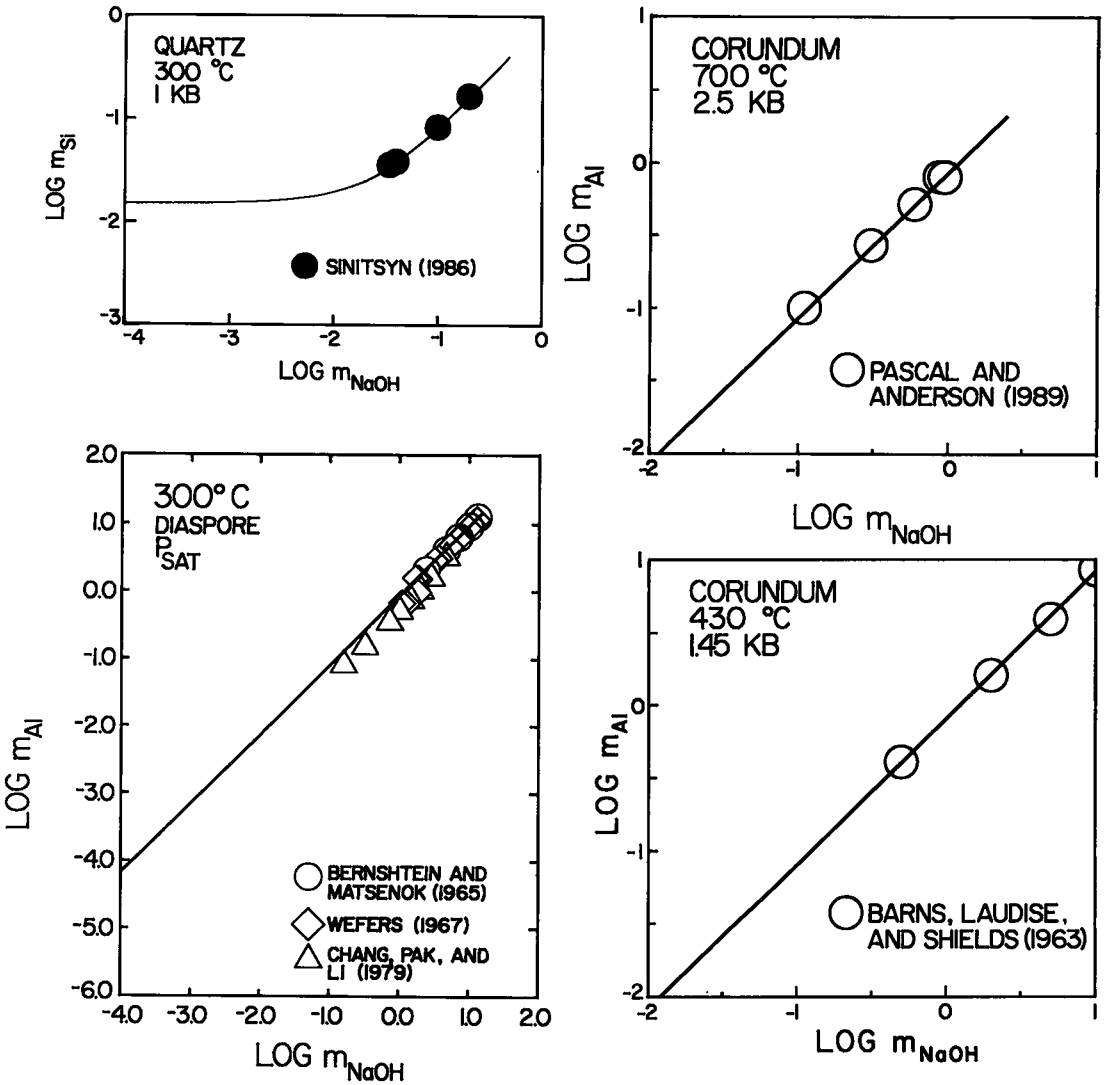

FIG. 3. Solubilities of corundum, diaspore, and quartz in NaOH solutions at various elevated pressures and temperatures. The symbols represent experimental data taken from the literature, but the curves were generated independently assuming $b_{\gamma,NaOH^\circ} \approx b_{\gamma,NaCl^\circ}$ using equations given in Appendixes A and B, together with equations of state parameters, activity coefficients, and thermodynamic properties of the minerals and aqueous species at 25°C and 1 bar taken from Pokrovskii & Helgeson (1989), Oelkers & Helgeson (1991a), Pokrovskii *et al.* (1991), and V.A. Pokrovskii & H.C. Helgeson (in prep.).

parts. Similar agreement is apparent in Figure 3, where the solubilities of corundum, diaspore, and quartz in NaOH solutions are plotted as a function of the molality of NaOH at various high temperatures and pressures. These observations, together with the fact that the curves in Figure 3 were generated independently of the experimental data represented by the symbols, strongly support the validity and generality of the equations and thermodynamic data used to calculate the mineral solubilities depicted in the bulk composition - pH diagrams discussed below.

The apparent standard partial molal Gibbs free energies of formation of minerals used in the solubility calculations described in the present study were calculated as functions of temperature and pressure from Eqns. (A1) and (A2) in Appendix A using values of the standard partial molal ther-

modynamic properties of the minerals at 25°C and 1 bar generated by V.A. Pokrovskii & H.C. Helgeson (in prep.). Taking account of the difference in the reference standard partial molal enthalpy of formation from the elements of corundum adopted in the two studies, the values of these properties are closely consistent with those at 25°C and 1 bar retrieved by Helgeson *et al.* (1978). Values of the activity of H_2O were computed from osmotic coefficients of NaCl solutions generated from equations and parameters taken from Helgeson *et al.* (1981), Oelkers & Helgeson (1990), and Pokrovskii *et al.* (1991), which yield values that are closely consistent with those generated by Pitzer *et al.* (1984). The activity coefficients of aqueous species used to calculate the mineral solubilities summarized in the following pages were computed in the manner described in Appendix B. The dependence of these solubilities on bulk composition and solution pH are discussed in subsequent pages in the context of reactions among minerals and aqueous solutions in geochemical processes.

The bulk composition – pH diagrams described below were generated by computing the solubilities of minerals in either 0.01 *m* or 1.0 *m* NaCl solutions containing either HCl or NaOH concentrations consistent with values of solution pH ranging from 0 to 12 at 25°, 200°, and 300°C at P_{SAT}, which represents pressures corresponding to liquid–vapor equilibrium for the system H_2O, except at temperatures less than 100°C, where it refers to the reference pressure of 1 bar. Accordingly, the effective ionic strength of the aqueous phase is a dependent variable, as is the activity of H_2O. The calculations were carried out with the aid of computer code PHX (Molchanov 1988), which was used to locate the boundaries of the stability fields as a function of η_c and solution pH by solving simultaneously statements of the law of mass action and material-balance equations for specified values of η_c and pH. The reaction paths represented by the dashed lines with arrows in the η_c – pH diagrams were generated using the Gibbs free energy minimization code named GIBBS (Shvarov 1981). For the sake of simplicity and clarity in demonstrating the application of these diagrams to hydrothermal systems, only equilibrium solubilities of stoichiometric minerals that are thermodynamically stable were considered in the calculations. Metastable phase-relations, solid solutions such as illite and smectite, multiple reactants, and the effect of the pH dependence of reaction rates and activation energies on reaction paths and nonequilibrium mineral solubilities will be considered in subsequent communications. The abbreviations of mineral names used in the present communication to designate the stability fields of stoichiometric minerals in the bulk composition – pH diagrams described below were taken from Kretz (1983). These are: Ab albite, Anl analcite, Dsp diaspore, Kln kaolinite, Kfs K-feldspar, Kls kalsilite, Ms muscovite, Ne nepheline, Prl pyrophyllite, and Qtz quartz. The terms *albite* and *K-feldspar* refer to the stoichiometric minerals in their stable states of order–disorder at any pressure and temperature (Helgeson *et al.* 1978).

Hydrolysis of kaolinite at 25°C and 1 bar

To illustrate the advantages of simultaneously describing mineral solubilities and the consequences of reactions among minerals and aqueous solutions in terms of η_c, an $\eta_{Al_2Si_2O_5(OH)_4}$ — pH diagram is depicted in Figure 4 for the system Al_2O_3–SiO_2–HCl–NCl–NaOH–H_2O at 25°C, 1 bar, and m_{NaCl} = 0.01. As indicated above, the components HCl and NaOH are included in this system (as well as those considered below) in order to independently vary solution pH. The boundaries of the stability fields, other than those that are vertical in Figure 4, represent mineral solubilities. The reactions represented by the stability-field boundaries in this figure are listed in Table 3. The dashed reaction-paths labeled *abcd*, *efg*, and *hijk* in Figure 4 represent the consequences of the reaction of kaolinite with 0.01 *m* NaCl solutions in open systems in which the values of pH are buffered by flowing fluids and equal to those at *a*, *e*, and *h*. These reaction paths are discussed in later pages.

It can be deduced from Figure 4 that kaolinite dissolves congruently at 25°C and 1 bar at values of pH between 3.73 and 4.27 in accord with reaction (3-3). [In the two-digit reaction numbers cited in the text, the first digit refers to the table in which the reaction occurs, and the second, to the numerical sequence of the reaction in the table.] In more acid solutions, kaolinite dissolves incongruently to form quartz. At values of pH greater than 4.27, diaspore is the first mineral to precipitate from solution, which occurs over a wide range of solution pH from 4.27 to 12.

The values of log $\eta_{Al_2Si_2O_5(OH)_4}$ represented by the stability-field boundaries in Figure 4 can be used to compute the total molalities of Al and Si by adding the logarithm of the number of moles of Al and Si, respectively, in one mole of kaolinite (2) to the values of η_c on the ordinate. Although the total molality of silica in the aqueous phase coexisting with kaolinite and quartz at values of pH less than 3.73 is controlled by the solubility of quartz, the total molality of Al is controlled by the equilibrium constant for reaction (3-2). In solu-

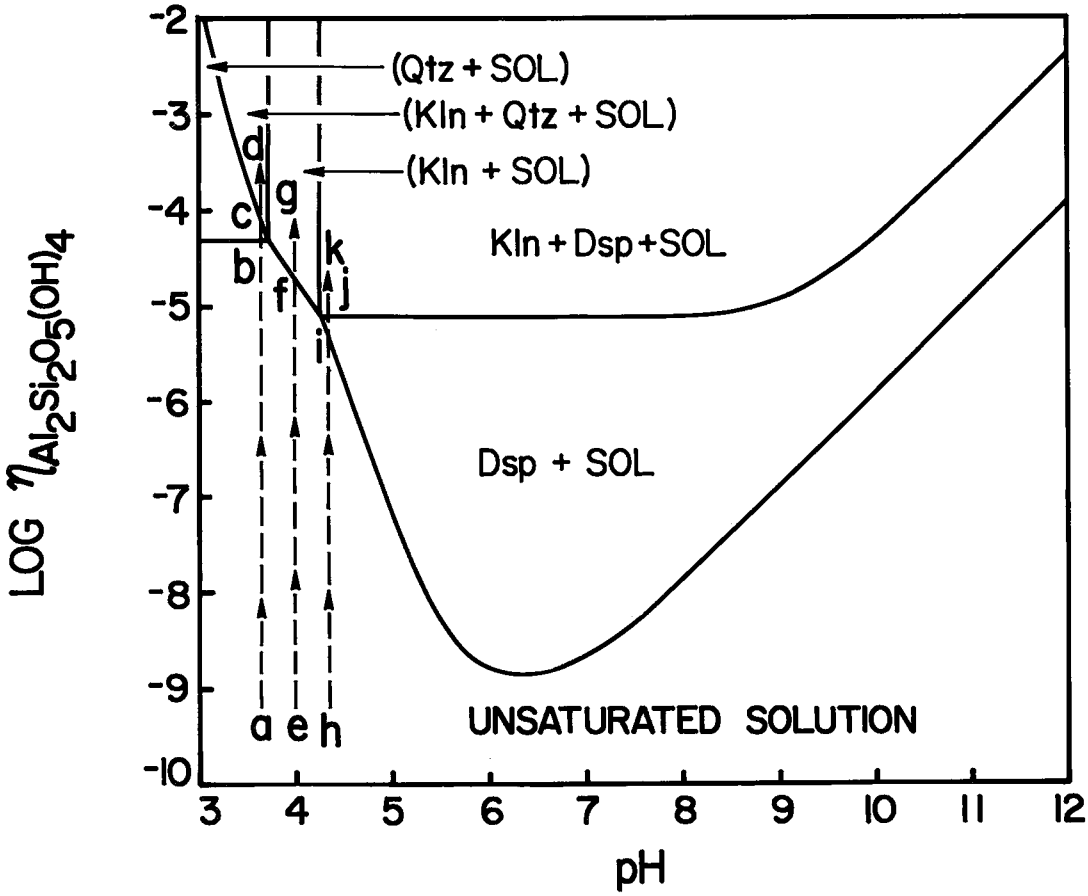

FIG. 4. $\eta_{Al_2Si_2O_5(OH)_4}$ — pH diagram for the system Al_2O_3–SiO_2–HCl–NaCl–NaOH–H_2O at 25°C, and m_{NaCl} = 0.01 (see text). The annotated reaction-paths represented by the dashed lines with arrows at pH 3.65, 4.00, and 4.35, correspond to those shown in Figure 5. These reaction paths are a consequence of the irreversible reaction of kaolinite in an open system with 0.01 m_{NaCl} solutions in which the values of pH are buffered by flowing fluids.

TABLE 3. REACTIONS REPRESENTING THE STABILITY FIELD BOUNDARIES DEPICTED IN FIG. 4.

REACTION NUMBER	REACTION[a]	pH RANGE[b]
(3–1)	$SiO_2^\circ \rightleftarrows SiO_2$ (quartz)	2 – 3.5
(3–2)	$2\ SiO_2$ (quartz) $+ 2Al^{3+} + 5H_2O \rightleftarrows Al_2Si_2O_5(OH)_4$ (kaolinite) $+ 6H^+$	2 – 3.5
(3–3)	$2Al^{3+} + 2SiO_2^\circ + 5H_2O \rightleftarrows Al_2Si_2O_5(OH)_4$ (kaolinite) $+ 6H^+$	3.73 – 4.27
(3–4)	$Al(OH)_{3-n}^n + (n-1)H_2O \rightleftarrows AlO(OH)$ (diaspore) $+ nH^+$; $(n = -1,\ldots,3)$	4.27 – 12
(3–5a)	$2AlO(OH)$ (diaspore) $+ 2SiO_2^\circ + H_2O \rightleftarrows Al_2Si_2O_5(OH)_4$ (kaolinite)	4.27 – 8.5
(3–5b)	$2AlO(OH)$ (diaspore) $+ 2H_3SiO_4^- + 2H^+ \rightleftarrows Al_2Si_2O_5(OH)_4$ (kaolinite) $+ 3H_2O$	8.5 – 12

[a]The aqueous aluminum and silica species shown in these reactions are those that predominate in the pH–range shown on the right side of the table. [b]The pH–range refers to the pH limits of the stability field boundaries depicted in the figure.

tions saturated with both kaolinite and diaspore, the total molality of aluminum is fixed by the solubility of diaspore in accord with reaction (3–4), but the total molality of Si is controlled by the equilibrium constants for reactions (3–5a) and (3–5b).

The slopes of the stability-field boundaries depicted in Figure 4 are determined by the dependence of the mineral solubilities on pH in the various ranges of pH in which the minerals are stable. For example, the slope of the quartz solubility curve is zero because $H_3SiO_4^-$ and its dissociation products form to negligible degrees in acid solutions. Hence, reaction (3–1) determines the solubility of quartz shown in the diagram. For the same reason, the solubility of kaolinite in the presence of diaspore is controlled by reaction (3–5a) until the pH increases sufficiently for $H_3SiO_4^-$ to form to appreciable degrees, and reaction (3–5b) then controls the pH dependence of the solubility of kaolinite. Accordingly, the solubility curve shown for kaolinite in the presence of diaspore in Figure 4 is essentially horizontal below a pH of approximately 9, and then increases with increasing pH. The minimum in the solubility curve for diaspore occurs in response to the successive predominance of aluminum hydroxide complexes with increasing pH as n increases in reaction (3–4).

The phase relations depicted in Figure 4 can be compared with those in the solubility diagrams

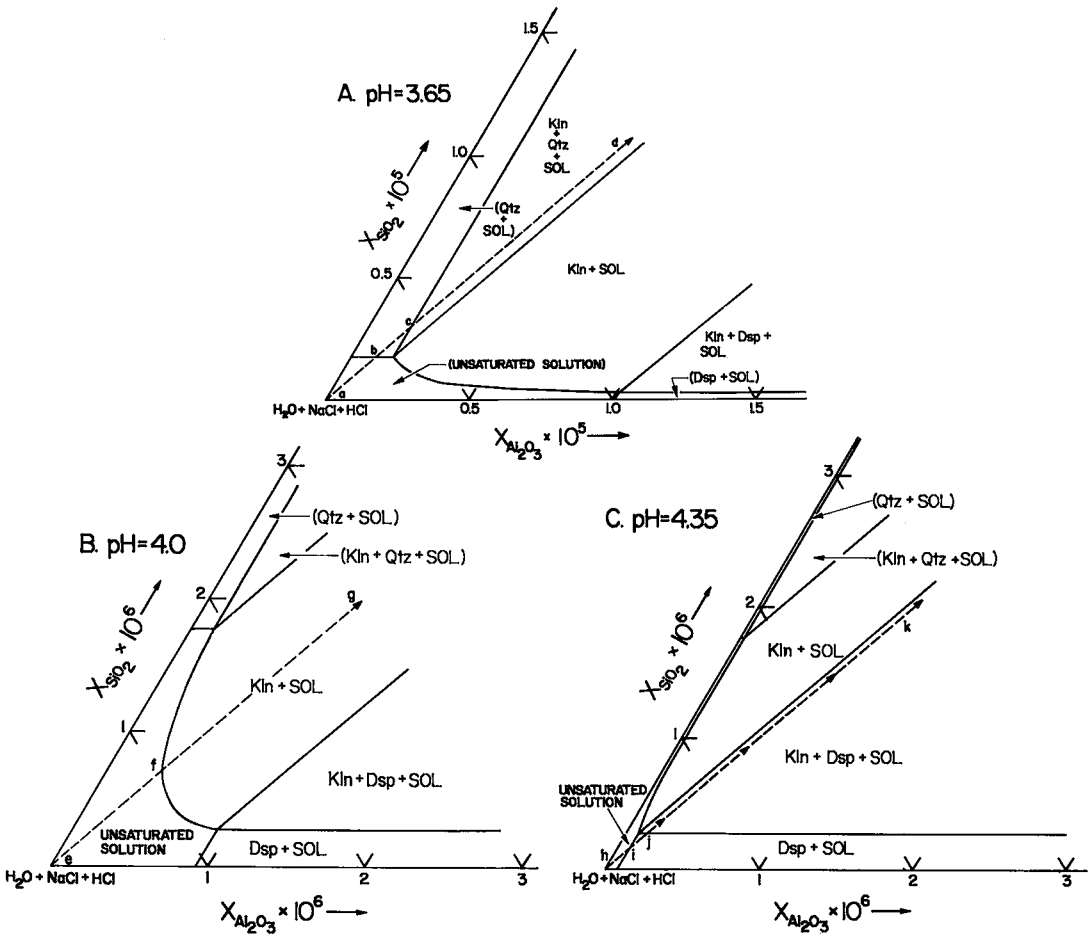

FIG. 5. Mineral solubilities and phase relations in the system Al_2O_3–SiO_2–HCl–NaCl–NaOH–H_2O as a function of the mole fractions of SiO_2 and Al_2O_3 in the system at 25°C, 1 bar, m_{NaCl} = 0.01, and constant values of the solution pH of 3.65 (diagram A), 4.00 (diagram B), and 4.35 (diagram C); see text. The annotated reaction-paths shown as dashed lines with arrows correspond to those depicted in Figure 4 (see caption of Fig. 4).

shown in Figure 5, where the mole fraction of SiO_2 (X_{SiO_2}) in the system is plotted against the mole fraction of Al_2O_3 ($X_{Al_2O_3}$) at 25°C, 1 bar, and constant values of solution pH of 3.65 (Fig. 5A), 4.00 (Fig. 5B), and 4.35 (Fig. 5C). The dashed reaction-paths with arrows labeled *abcd*, *efg*, and *hijk* in Figure 4 are similarly labeled in Figure 5. It can be deduced from Figures 4 and 5A that kaolinite dissolves congruently along reaction path *ab*. However, with continued dissolution along *bc*, a small amount of quartz is precipitated as a product of the incongruent reaction. The number of moles of quartz precipitated (kg H_2O)$^{-1}$ corresponds to twice the value of $\eta_{Al_2Si_2O_5(OH)_4}$ at point *c* minus twice that at point *b*. At point *c*, the aqueous phase reaches equilibrium with both quartz and kaolinite. Addition of more kaolinite to the system then causes the bulk composition to change toward point *d*, in accord with Eqn. (28).

In contrast to reaction path *abcd* in Figures 4 and 5A, kaolinite dissolves congruently until it reaches equilibrium with the aqueous phase along reaction path *efg* in Figures 4 and 5B. Note that the scale of the solubility diagram in Figure 5B is much larger than that of the diagram in Figure 5A, which is a consequence of the dramatic decrease in the total molality of Al in solutions that equilibrate with kaolinite as the solution pH increases from 3.65 to 4.00. At pH = 4.35 along reaction path *hijk* in Figures 4 and 5C, kaolinite dissolves incongruently to form diaspore along *ij*. At *j*, the aqueous phase reaches saturation with both diaspore and kaolinite. If kaolinite is subsequently added to the system, the bulk composition then changes along *jk* in accord with Eqn. (28). The dashed reaction-paths in Figures 5A, 5B, and 5C coincide with the position of the tie line between H_2O and kaolinite, which is not shown in the figures.

Hydrolysis of muscovite at 300°C and P_{SAT}

Phase relations in the system K_2O–Al_2O_3–SiO_2–HCl–NaCl–NaOH–H_2O are shown in Figure 6 as a function of $\eta_{KAl_3Si_3O_{10}(OH)_2}$ and pH in a 0.01 *m* NaCl solution at 300°C and P_{SAT}. The reactions

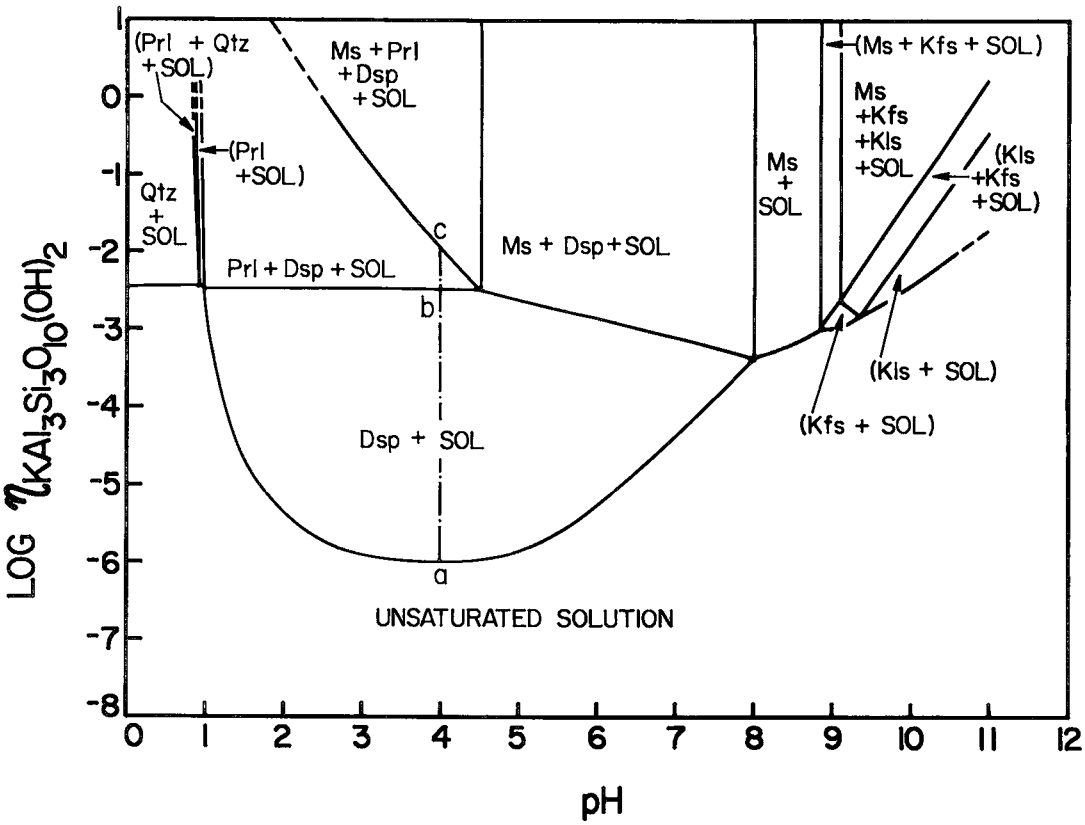

FIG. 6. $\eta_{KAl_3Si_3O_{10}(OH)_2}$ – pH diagram for the system K_2O–Al_2O_3–SiO_2–HCl–NaCl–NaOH–H_2O at 300°C, P_{SAT}, and m_{NaCl} = 0.01 (see text).

TABLE 4. REACTIONS REPRESENTING THE STABILITY FIELD BOUNDARIES DEPICTED IN FIG. 6.

REACTION NUMBER	REACTION[a]	pH RANGE[a]
(4–1)	$SiO_2^\circ \rightleftarrows SiO_2$ (quartz)	0 – 0.9
(4–2)	$4SiO_2$ (quartz) $+ 2Al^{3+} + 4H_2O \rightleftarrows Al_2Si_4O_{10}(OH)_2$ (pyrophyllite) $+ 6H^+$	0.84 – 0.9
(4–3)	$2Al^{3+} + 4SiO_2^\circ + 4H_2O \rightleftarrows Al_2Si_4O_{10}(OH)_2$ (pyrophyllite) $+ 6H^+$	0.9 – 0.98
(4–4)	$Al(OH)_{3-n}^n + (n-1)H_2O \rightleftarrows AlO(OH)$ (diaspore) $+ nH^+$; $(n=-1,...,3)$	0.98 – 8.0
(4–5)	$2AlO(OH)$ (diaspore) $+ 4SiO_2^\circ \rightleftarrows Al_2Si_4O_{10}(OH)_2$ (pyrophyllite)	0.98 – 4.5
(4–6)	$3Al_2Si_4O_{10}(OH)_2$ (pyrophyllite) $+ 6AlO(OH)$ (diaspore) $+ 4K^+ \rightleftarrows 4KAl_2(AlSi_3)O_{10}(OH)_2$ (muscovite) $+ 4H^+$	1.8 – 4.5
(4–7)	$3AlO(OH)$ (diaspore) $+ 3SiO_2^\circ + K^+ \rightleftarrows KAl_2(AlSi_3)O_{10}(OH)_2$ (muscovite) $+ H^+$	4.5 – 8.0
(4–8)	$K^+ + 3Al(OH)_4^- + 3SiO_2^\circ + 2H^+ \rightleftarrows KAl_2(AlSi_3)O_{10}(OH)_2$ (muscovite) $+ 6H_2O$	8.0 – 8.84
(4–9)	$K^+ + Al(OH)_4^- + 3SiO_2^\circ \rightleftarrows KAlSi_3O_8$ (K–feldspar) $+ 2H_2O$	8.84 –9.37
(4–10)	$KAlSi_3O_8$ (K–feldspar) $+ 2Al(OH)_4^- + 2H^+ \rightleftarrows KAl_2(AlSi_3)O_{10}(OH)_2$ (muscovite) $+ 4H_2O$	8.84 – 9.1
(4–11)	$K^+ + Al(OH)_4^- + SiO_2^\circ \rightleftarrows KAlSiO_4$ (kalsilite) $+ 2H_2O$	9.37 – 11
(4–12)	$KAlSiO_4$ (kalsilite) $+ 2SiO_2^\circ \rightleftarrows KAlSi_3O_8$ (K–feldspar)	9.37 – 11
(4–13)	$0.5KAlSiO_4$ (kalsilite) $+ 0.5KAlSi_3O_8$ (K–feldspar) $+ 2Al(OH)_4^- + 2H^+ + SiO_2^\circ \rightleftarrows KAl_2(AlSi_3)O_{10}(OH)_2$ (muscovite) $+ 4H_2O$	9.1 – 11

[a]See footnotes *a* and *b* of Table 2.

represented by the stability-field boundaries shown in this figure are listed in Table 4. It can be deduced from the curves depicted in Figure 6 that muscovite dissolves congruently in alkaline solutions with a pH between 8.0 and 8.84, which is consistent with experimental observations reported by Mukhamet-Galeyev *et al.* (1984). At a pH greater than 8.84, muscovite dissolves incongruently to form K-feldspar or kalsilite and K-feldspar.

The total molalities of potassium, aluminum, and silicon (m_K, m_{Al}, and m_{Si}, respectively) at any point in the bulk composition – pH diagram in Figure 6 can be computed from $\eta_{KAl_3Si_3O_{10}(OH)_2}$. For example, at a solution pH of 4, m_K at point *c* is equal to 10^{-2}, but m_{Al} and m_{Si} at point *c* are equal to $3 \times \eta_{KAl_3Si_3O_{10}(OH)_2}$ at point *a* and $3 \times \eta_{KAl_3Si_3O_{10}(OH)_2}$ at point *b*, respectively.

The order of precipitation of reaction products with increasing $\eta_{KAl_3Si_3O_{10}(OH)_2}$ in Figure 6 is determined by the equilibrium constants for the reactions in Table 4 and the extent to which the mineral solubilities shown in the figure depend on pH. At a pH less than 8.00 and and greater than 0.98, muscovite dissolves incongruently to form diaspore. As diaspore continues to precipitate at the expense of muscovite, the solution becomes saturated with respect to pyrophyllite if the solution pH is greater than 0.98 and less than 4.50. Continued dissolution of muscovite in this pH range finally results in equilibrium among muscovite, diaspore, pyrophyllite, and the aqueous phase. In highly acid solutions, quartz (at a pH 0.90) and pyrophyllite (at a pH between 0.90 and 0.98) are the first minerals to precipitate from solution as $\eta_{KAl_3Si_3O_{10}(OH)_2}$ increases.

Hydrolysis of K-feldspar at 200°C and P_{SAT}

The solubilities of minerals in the system K_2O–Al_2O_3–SiO_2–HCl–NaCl–NaOH–H_2O at 200°C and P_{SAT} in a 0.01 *m* NaCl solution are depicted in terms of $\eta_{KAlSi_3O_8}$ and pH in Figure 7. The reactions represented by the stability-field boundaries shown in this figure are listed in Table 5. It can be seen in Figure 7 that K-feldspar dissolves congruently over a short range of pH from 9.03 to 9.80. In more alkaline solutions, K-feldspar dissolves incongruently to form kalsilite.

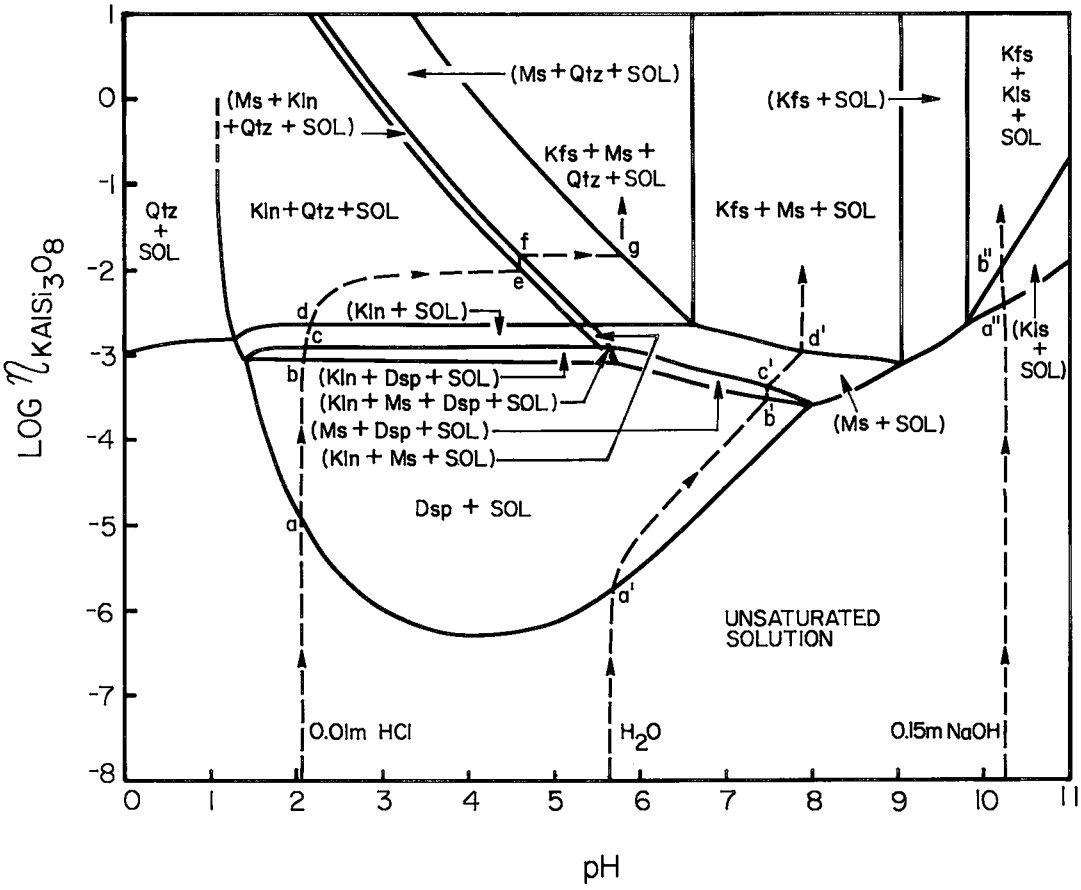

FIG. 7. $\eta_{KAlSi_3O_8}$ - pH diagram for the system K_2O-Al_2O_3-SiO_2-HCl-NaCl-NaOH-H_2O at 200°C, P_{SAT}, and m_{NaCl} = 0.01 (see text). The annotated reaction-paths corresponding to the dashed lines with arrows represent the conseqences of the irreversible dissolution in a closed system of K-feldspar in 0.01 m_{NaCl} solutions with different initial values of pH.

In less alkaline solutions, the identities and relative amounts of the minerals that form as intermediate reaction-products during the dissolution of K-feldspar are primarily determined by the initial pH of the aqueous phase. For example, it can be deduced from Figure 7 that reaction of K-feldspar with an acid aqueous solution with an initial pH of 2.08 in a closed system causes precipitation of diaspore along reaction path *ab*. The number of moles of diaspore precipitated (kg H_2O)$^{-1}$ corresponds to the value of $\eta_{KAlSi_3O_8}$ at point *b* minus that at point *a*. At the stage of reaction progress represented by *b* in Figure 7, kaolinite begins to precipitate at the expense of diaspore in accord with reaction (5-5), which continues until the solution reaches composition *c*, where no diaspore remains in the system. The number of moles of kaolinite (kg H_2O)$^{-1}$ precipitated along reaction path *bc* is equal to one half $\eta_{KAlSi_3O_8}$ at point *c* minus one half that at point *b*. As K-feldspar continues to dissolve, kaolinite precipitates along *cd* until the solution becomes saturated with quartz at *d*. Kaolinite and quartz then coprecipitate along segment *de* as the solution pH increases and reaches *e*, where muscovite becomes a stable phase. The number of moles of kaolinite (kg H_2O)$^{-1}$ precipitated along reaction path *de* is equal to one half $\eta_{KAlSi_3O_8}$ at point *e* minus one half that at point *d*. In contrast, the number of moles of quartz (kg H_2O)$^{-1}$ precipitated along reaction path *de* is equal to one third the difference between $\eta_{KAlSi_3O_8}$ at point *e* minus the sum of one half of the number of moles of kaolinite (log H_2O)$^{-1}$ precipitated and the equilibrium solubility of quartz. Along reaction-path segment *ef* in Figure 7, kaolinite reacts with the aqueous phase to form muscovite until all of

TABLE 5. REACTIONS REPRESENTING THE STABILITY FIELD BOUNDARIES DEPICTED IN FIG. 7.

REACTION NUMBER	REACTION[a]	pH RANGE[a]
(5–1)	$SiO_2^\circ \rightleftarrows \underset{\text{(quartz)}}{SiO_2}$	0 – 6.6
(5–2)	$\underset{\text{(quartz)}}{2SiO_2} + 2Al^{3+} + 5H_2O \rightleftarrows \underset{\text{(kaolinite)}}{Al_2Si_2O_5(OH)_4} + 6H^+$	1.1 – 1.3
(5–3)	$2Al^{3+} + 2SiO_2^\circ + 5H_2O \rightleftarrows \underset{\text{(kaolinite)}}{Al_2Si_2O_5(OH)_4} + 6H^+$	1.3 – 1.4
(5–4)	$Al(OH)_{3-n}^n + (n-1)H_2O \rightleftarrows \underset{\text{(diaspore)}}{AlO(OH)} + nH^+ ;\ (n=-1,\ldots,3)$	1.4 – 8.0
(5–5)	$\underset{\text{(diaspore)}}{2AlO(OH)} + 2SiO_2^\circ + H_2O \rightleftarrows \underset{\text{(kaolinite)}}{Al_2Si_2O_5(OH)_4}$	1.4 – 5.7
(5–6)	$\underset{\text{(kaolinite)}}{3Al_2Si_2O_5(OH)_4} + 2K^+ \rightleftarrows \underset{\text{(muscovite)}}{2KAl_2(AlSi_3)O_{10}(OH)_2} + 2H^+ + 3H_2O$	2.13 – 5.7
(5–7)	$\underset{\text{(muscovite)}}{KAl_2(AlSi_3)O_{10}(OH)_2} + \underset{\text{(quartz)}}{6SiO_2} + 2K^+ \rightleftarrows \underset{\text{(K–feldspar)}}{3KAlSi_3O_8} + 2H^+$	3.35 – 6.6
(5–8)	$\underset{\text{(diaspore)}}{3AlO(OH)} + 3SiO_2^\circ + K^+ \rightleftarrows \underset{\text{(muscovite)}}{KAl_2(AlSi_3)O_{10}(OH)_2} + H^+$	5.7 – 8
(5–9)	$\underset{\text{(muscovite)}}{KAl_2(AlSi_3)O_{10}(OH)_2} + 2K^+ + 6SiO_2^\circ \rightleftarrows \underset{\text{(K–feldspar)}}{3KAlSi_3O_8} + 2H^+$	6.6 – 9.03
(5–10)	$K^+ + 3Al(OH)_4^- + 3SiO_2^\circ + 2H^+ \rightleftarrows \underset{\text{(muscovite)}}{KAl_2(AlSi_3)O_{10}(OH)_2} + 6H_2O$	8.0 – 9.03
(5–11)	$K^+ + Al(OH)_4^- + 3SiO_2^\circ \rightleftarrows \underset{\text{(K–feldspar)}}{KAlSi_3O_8} + 2H_2O$	9.03 – 9.8
(5–12)	$K^+ + Al(OH)_4^- + SiO_2^\circ \rightleftarrows \underset{\text{(kalsilite)}}{KAlSiO_4} + 2H_2O$	9.8 – 11.0
(5–13)	$\underset{\text{(kalsilite)}}{KAlSiO_4} + 2SiO_2^\circ \rightleftarrows \underset{\text{(K–feldspar)}}{KAlSi_3O_8}$	9.8 – 11.0

[a]See footnotes *a* and *b* of Table 2.

the kaolinite is consumed at point *f*. Muscovite and quartz then coprecipitate along *fg* until point *g* is reached, where the aqueous phase achieves equilibrium with K-feldspar.

The logarithm of the number of moles of minerals produced and destroyed (kg $H_2O)^{-1}$ (n_ϕ) along reaction path *abcdefg* in Figure 7 is depicted as a function of $\eta_{KAlSi_3O_8}$ in Figure 8. The curve for K-feldspar shown in this figure represents the consequences of adding K-feldspar to the system in accord with Eqn. (28) along the path above *g* in Figure 7. It can be seen in Figure 8 that the reaction process described above leads to precipitation (kg $H_2O)^{-1}$ of 0.005 moles of muscovite and 0.025 moles of quartz at the expense of 0.016 moles of K-feldspar.

The sequence of events along reaction path *abcdefg* in Figure 7 is quite different from those along paths *a'b'c'd'* and *a"b"*. As K-feldspar dissolves in a closed system along reaction path *a'b'c'd'*, kaolinite and quartz fail to appear as intermediate reaction-products because their stability fields are restricted to more acid solutions. In highly alkaline solutions along path *a"b"*, kalsilite appears as a product of incongruent reaction at point *a"* and continues to precipitate along reaction-path segment *a"b"* until the solution reaches equilibrium with K-feldspar.

The release of K_2O into the aqueous phase during the dissolution of K-feldspar displaces the hydrolysis reaction represented by

$$K_2O + 2H^+ \rightleftarrows 2K^+ + H_2O \qquad (29)$$

to the right, which favors increasing pH. However, the reaction paths are affected dramatically by this reaction only if $-\log \eta_{KAlSi_3O_8} \geq$ pH. Precipitation of products of incongruent reactions, such as muscovite at the expense of kaolinite in accord with reaction (5–6), is accompanied by the release of hydrogen ions. The two opposing processes that favor increasing and decreasing pH, respectively (*i.e.*, release of K_2O into solution as a result of the dissolution of K-feldspar and release of H^+ during precipitation of reaction products), compete with each other during the dissolution process, which may lead to complex changes in pH along the reaction path.

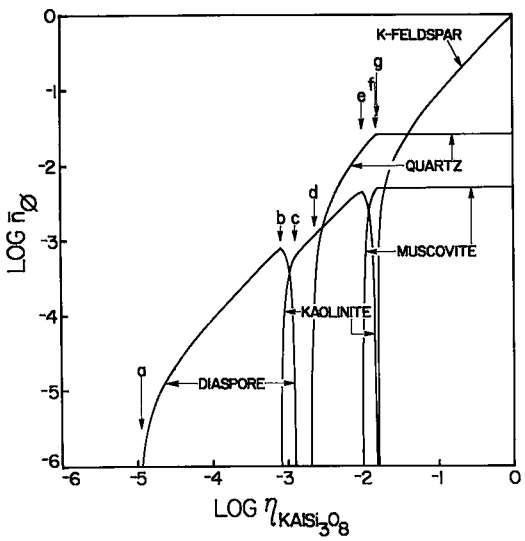

FIG. 8. Moles of minerals precipitated and dissolved (kg $H_2O)^{-1}$ ($\bar{n}_{\phi}$) as a function of bulk composition during the incongruent reaction of K-feldspar with the aqueous phase along reaction path *abcdefg* in Figure 7 (see text and caption of Fig. 7).

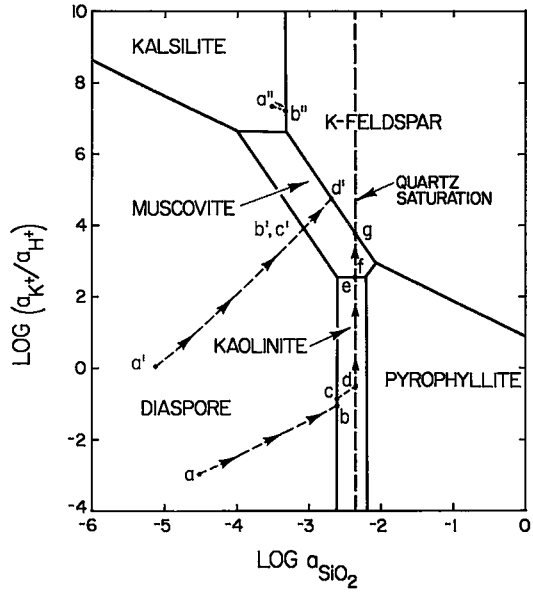

FIG. 9. Activity diagram for the system K_2O–Al_2O_3–SiO_2–HCl–H_2O at 200°C and P_{SAT} (see text). The annotated reaction-paths represented by the dashed lines with arrows correspond to those shown in Figure 7.

The reaction paths shown in Figure 7 are also plotted on the activity diagram depicted in Figure 9, where it can be seen that a_{K^+}/a_{H^+} in the aqueous phase increases to a greater degree along reaction path *a'b'* than it does along *ab*, which results in the large increase in pH along *a'b'* in Figure 7. Because the solution pH is low along path *ab*, precipitation of diaspore along this path has little influence on solution pH. Taken together, diagrams like those shown in Figures 7–9 afford comprehensive and quantitative description of phase relations in hydrothermal systems before,

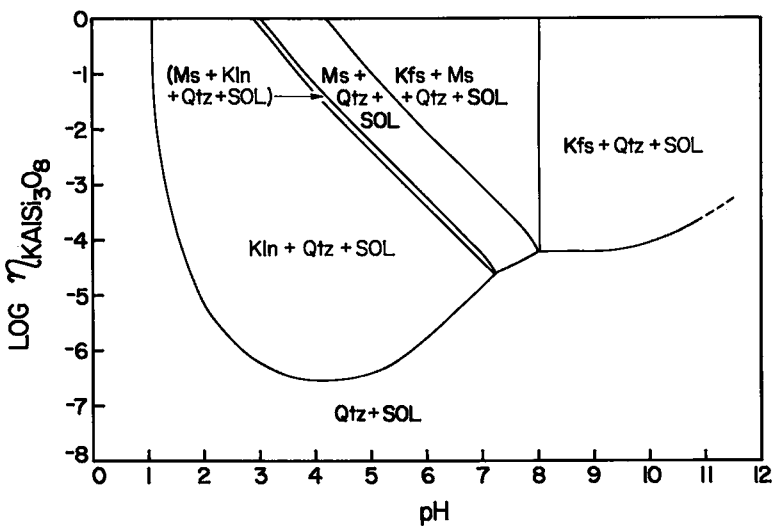

FIG. 10. $\eta_{KAlSi_3O_8}$– pH diagram for the system K_2O–Al_2O_3–SiO_2–HCl–NaCl–NaOH–H_2O at 200°C, P_{SAT}, and m_{NaCl} = 0.01 in an aqueous solution coexisting with quartz (see text).

during, and after irreversible reaction of a given mineral or mineral assemblage with the aqueous phase.

Reaction paths *abcdefg*, *a'b'c'd'*, and *a"b"* in Figures 7 and 9 represent the evolution of solution pH in a closed system with a given bulk-composition. However, if the system is open, the pH of the aqueous solution may change independently of chemical processes that occur in the system. Changes in solution pH in open systems can be caused by dilution of hydrothermal fluids with groundwater or mixing of fluids of different composition due to reopening of fissures and other processes. In the laboratory, similar changes can be imposed by the "pH-stat" technique to change pH over a wide range at any given value of η_c. Under these circumstances, the mineralogical consequences may be quite different than those resulting from the hydrolysis of K-feldspar in a closed system. For example, if the solution pH is independently increased from point *g* in Figure 7 at constant $\eta_{KAlSi_3O_8}$, the mass of K-feldspar increases in accord with reaction (5-7), which proceeds until all of the quartz in the system is consumed. Further increase in pH then leads to consumption of muscovite in accord with reaction (5-9) until it completely disappears at pH = 9.03, where equilibrium is achieved between K-feldspar and the aqueous phase.

The consequences of the dissolution of K-feldspar in an aqueous phase that is saturated with quartz at 200°C and P_{SAT} can be assessed in Figure 10. Because equilibrium with quartz reduces considerably the number of mineral stability-fields in the system, kaolinite is the first mineral to precipitate from solution during the dissolution of K-feldspar in solutions saturated with quartz at pH less than 7.2 in Figure 10. Kaolinite is followed by muscovite and, finally, by equilibrium with K-feldspar, which dissolves congruently in the presence of quartz only if the solution pH shown in Figure 10 is greater than 8.

Hydrolysis of albite at 200°C and P_{SAT}

The analog of Figure 7 depicting mineral solubilities in a 0.01 *m* NaCl solution for the system K_2O–Al_2O_3–SiO_2–HCl–NaOH–H_2O at 200°C and P_{SAT} is shown in Figure 11 for the system Na_2O–Al_2O_3–SiO_2–HCl–NaCl–NaOH–H_2O. The chemical reactions represented by the stability-field boundaries in Figure 11 are listed in Table 6. Comparison of Figures 7 and 11 indicates that the configurations of the stability fields on the left sides of the diagrams are almost identical, but those on the right sides are somewhat different. These differences arise primarily from the appearance of a stability field for analcite at values of pH in excess of 8.10 in Figure 11. It can be deduced from Figure 11 that analcite forms as a product of incongruent reaction during hydrolysis of albite in alkaline solutions, which is consistent

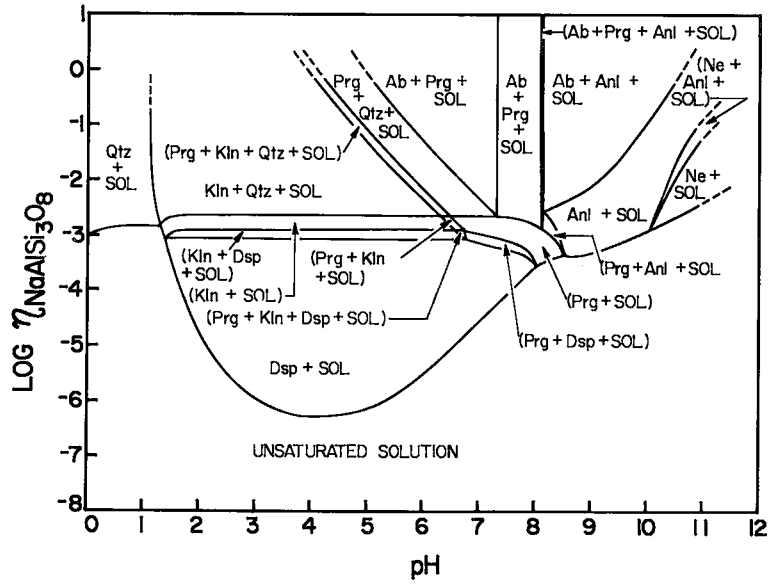

FIG. 11. $\eta_{NAlSi_3O_8}$– pH diagram for the system Na_2O–Al_2O_3–SiO_2–HCl–NaCl–NaOH–H_2O at 200°C, P_{SAT}, and m_{NaCl} = 0.01 (see text).

TABLE 6. REACTIONS REPRESENTING THE STABILITY FIELD BOUNDARIES DEPICTED IN FIG. 11.

REACTION NUMBER	REACTION[a]	pH RANGE[a]
(6–1)	$SiO_2^\circ \rightleftarrows SiO_2$ (quartz)	0 – 7.32
(6–2)	$2SiO_2$ (quartz) $+ 2Al^{3+} + 5H_2O \rightleftarrows Al_2Si_2O_5(OH)_4$ (kaolinite) $+ 6H^+$	1.1 – 1.3
(6–3)	$2Al^{3+} + 2SiO_2^\circ + 5H_2O \rightleftarrows Al_2Si_2O_5(OH)_4$ (kaolinite) $+ 6H^+$	1.3 – 1.4
(6–4)	$Al(OH)_{3-n}^n + (n-1)H_2O \rightleftarrows AlO(OH)$ (diaspore) $+ nH^+$; $(n=-1,\ldots,3)$	1.2 – 8.0
(6–5)	$2AlO(OH)$ (diaspore) $+ 2SiO_2^\circ + H_2O \rightleftarrows Al_2Si_2O_5(OH)_4$ (kaolinite)	1.4 – 6.78
(6–6)	$3Al_2Si_2O_5(OH)_4$ (kaolinite) $+ 2Na^+ \rightleftarrows 2NaAl_2(AlSi_3)O_{10}(OH)_2$ (paragonite) $+ 2H^+ + 3H_2O$	3.7 – 6.78
(6–7)	$NaAl_2(AlSi_3)O_{10}(OH)_2$ (paragonite) $+ 6SiO_2$ (quartz) $+ 2Na^+ \rightleftarrows 3NaAlSi_3O_8$ (albite) $+ 2H^+$	4.7 – 7.32
(6–8)	$3AlO(OH)$ (diaspore) $+ 3SiO_2^\circ + Na^+ \rightleftarrows NaAl_2(AlSi_3)O_{10}(OH)_2$ (paragonite) $+ H^+$	6.78 – 8.0
(6–9)	$NaAl_2(AlSi_3)O_{10}(OH)_2$ (paragonite) $+ 2Na^+ + 6SiO_2^\circ \rightleftarrows 3NaAlSi_3O_8$ (albite) $+ 2H^+$	7.32 – 8.1
(6–10)	$Na^+ + 3Al(OH)_4^- + 3SiO_2^\circ + 2H^+ \rightleftarrows NaAl_2(AlSi_3)O_{10}(OH)_2$ (paragonite) $+ 6H_2O$	8.0 – 8.52
(6–11)	$NaAl_2(AlSi_3)O_{10}(OH)_2$ (paragonite) $+ 5H_2O \rightleftarrows NaAlSi_2O_6 \cdot H_2O$ (analcite) $+ 2Al(OH)_4^- + SiO_2^\circ + 2H^+$	8.1 – 8.52
(6–12)	$NaAlSi_2O_6 \cdot H_2O$ (analcite) $+ SiO_2^\circ \rightleftarrows NaAlSi_3O_8$ (albite) $+ H_2O$	8.12 – 11.0
(6–13)	$Na^+ + Al(OH)_4^- + 2SiO_2^\circ \rightleftarrows NaAlSi_2O_6 \cdot H_2O$ (analcite) $+ H_2O$	8.52 – 10.06
(6–14)	$Na^+ + Al(OH)_4^- + SiO_2^\circ \rightleftarrows NaAlSiO_4$ (nepheline) $+ 2H_2O$	10.06 – 11.0
(6–15)	$NaAlSiO_4$ (nepheline) $+ SiO_2^\circ + H_2O \rightleftarrows NaAlSi_2O_6 \cdot H_2O$ (analcite)	10.06 – 11.0

[a]See footnotes *a* and *b* of Table 2.

with experimental observations reported by Apps & Neil (1983). As a consequence, no monomineralic saturation-curve for albite appears in the diagram. Albite thus dissolves incongruently over the whole range of pH shown in Figure 11. Note that the stability field of nepheline is restricted to values of pH $\geq$ 10.06. As $\eta_{NaAlSi_3O_8}$ increases at these high values of pH, nepheline reacts with the aqueous phase to form analcite in accord with reaction (6–15). It can also be seen by comparison of Figures 7 and 11 that the stability fields of paragonite and albite occur at higher values of $\eta_{NaAlSi_3O_8}$ than the values of $\eta_{KAlSi_3O_8}$ corresponding to the stability fields of muscovite and K-feldspar. For example, at pH = 5, the molality of K required to precipitate muscovite in the presence of kaolinite and quartz is $\geq 10^{-2.40}$, but the molality of Na required for precipitation of paragonite is $\geq 10^{-1.30}$. At any pH, albite is a more soluble mineral than K-feldspar.

The effect of increasing the total molality of NaCl on the phase relations shown for a 0.01 *m* NaCl solution in Figure 11 can be assessed by comparing this figure with Figure 12, which was generated for a 1 *m* NaCl solution at 200°C and P_{SAT}. It can be deduced from comparison of these two figures that increasing m_{NaCl} expands the stability fields of paragonite, albite, nepheline, and analcite, which are then stable at lower values of $\eta_{NaAlSi_3O_8}$ and pH. Note that the values of $\eta_{NaAlSi_3O_8}$ corresponding to the lower limits of quartz stability in Figure 12 are slightly lower than they are in Figure 11, which is a consequence of the increase in $\bar{\gamma}_{SiO_2}$ in the more concentrated NaCl solution considered in Figure 12. Comparison of Figures 11 and 12 also reveals that the stability fields representing paragonite + kaolinite + quartz, albite + paragonite + quartz, and albite + paragonite + analcite at log $\eta_{NaAlSi_3O_8}$ less than –1

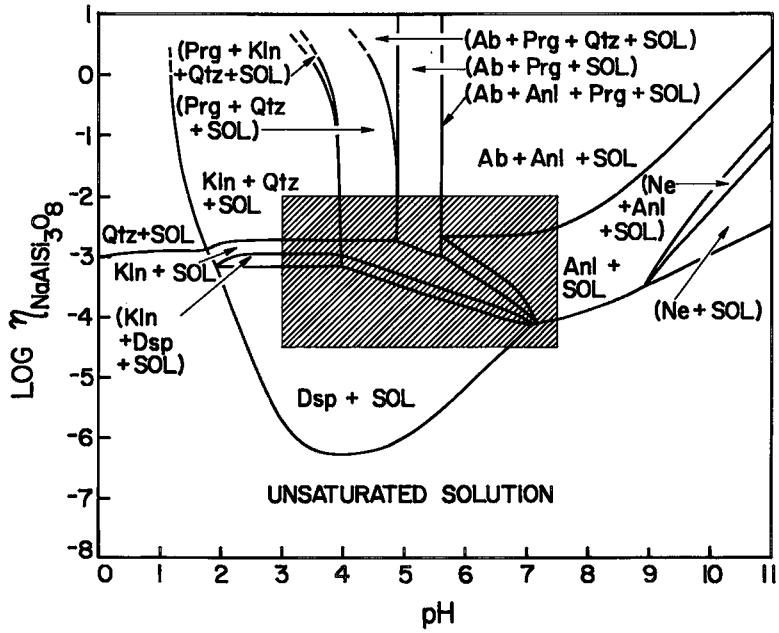

FIG. 12. $\eta_{NaAlSi_3O_8}$ – pH diagram for the system Na_2O–Al_2O_3–SiO_2–HCl–NaCl–NaOH–H_2O at 200°C, P_{SAT}, and m_{NaCl} = 1. The shaded area of the diagram is enlarged in Figure 13.

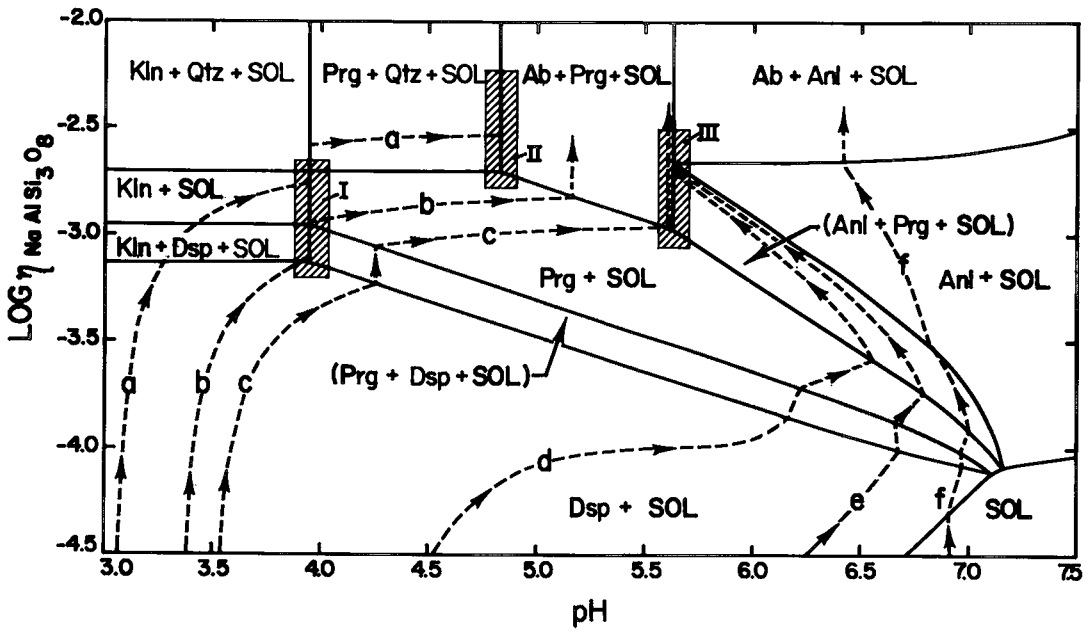

FIG. 13. Enlargement of the shaded area in Figure 12 with annotated reaction-paths represented by the dashed lines with arrows. The reaction paths are a consequence of the irreversible dissolution in a closed system of albite in 1 m_{NaCl} solutions with different initial values of solution pH (see text). The shaded areas labeled I, II, and III are enlarged in Figure 14.

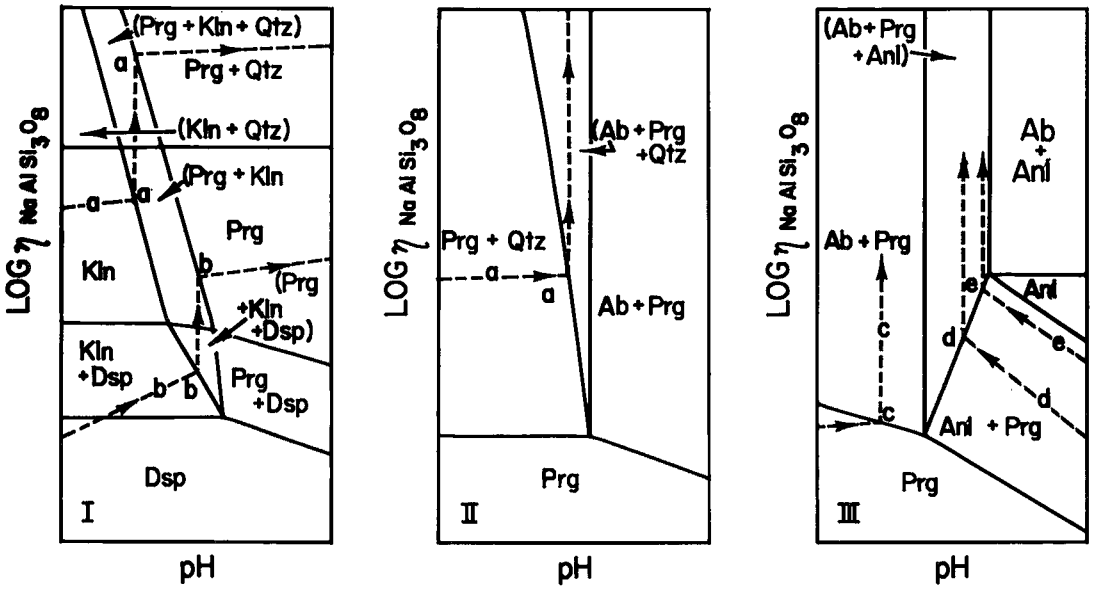

FIG. 14. Schematic enlargements of the shaded areas labeled I, II, and III in Figure 13 (see text). The reaction paths represented by the dashed lines with arrows correspond to those shown in Figure 13 (see caption of Fig. 13).

shrink with increasing m_{Na^+} and become indistinguishable from stability-field boundaries at the scale of the phase diagram depicted in Figure 11.

The shaded area in Figure 12 is enlarged in Figure 13, where a series of dashed reaction-paths labeled *a*, *b*, *c*, *d*, *e*, and *f* are shown to illustrate the consequences of the reaction of albite in a closed system with aqueous solutions with different initial values of pH on the identities and order of appearance of reaction products that appear in response to albite dissolution in a 1 molal NaCl solution. Reaction paths *a*, *b*, *c*, and *d* in Figure 13 were generated for molalities of HCl of 0.002, 0.001, 0.0007, and 0.0001, respectively. Path *e* results from reaction of albite with a 1 *m* NaCl solution (no acid or base added), but path *f* is a consequence of reaction with an initial solution in which the molality of NaOH is 0.0001. It can be seen in Figure 13 that all but one of the reaction paths result in final values of pH that are within the range 4.8–5.6, despite the much larger differences among the initial values of pH of the solutions, which range from 3.05 for path *a* to 6.25 for path *e*. The shaded insets labeled I, II, and III in Figure 13 are enlarged in Figure 14. The phase relations shown in the diagrams depicted in Figure 14 are schematic because they all fall within a pH range of 0.001. Hence, the mineral assemblages represented by the stability fields in Figure 14 are essentially pH buffers in concentrated solutions of sodium chloride.

CONCLUDING REMARKS

The calculations summarized above indicate that aluminosilicates such as kaolinite, muscovite, and K-feldspar dissolve congruently at the pressures and temperatures considered in the present study only in aqueous solutions with a pH that falls in relatively narrow ranges. Beyond these limits, and over the whole pH range in the case of albite, aluminosilicates dissolve incongruently to form other minerals. The relative amounts and stoichiometries of the reaction products depend on the solution pH. Adopting an approach similar to that used by Frisch & Helgeson (1984), compositional data can be used together with field observations of phase relations and η_c – pH diagrams like those discussed above to assess reaction paths and the pH of the aqueous phase involved in metasomatic processes. Although reactions involving only one reactant mineral were considered in the present study, plans call for generating comprehensive η_c – pH diagrams for systems involving solid solutions and two or more reactant minerals with and without kinetically controlled rates of reaction for a variety of compositions of aqueous solutions, at pressures and temperatures ranging from 25°C and 1 bar to 1000°C and 5 kbar.

Although the solubility diagrams discussed in the preceding pages were generated for relatively low temperatures ($\leq$300°C) at P_{SAT}, the same approach

can be applied to prediction and interpretation of phase relations at much higher temperatures and pressures. However, provision must be included in the calculations for many aqueous species that do not form to appreciable degrees at lower temperatures and pressures. For example, conductance data, electrostatic theory, and statistical mechanical calculations all indicate that triple ions such as K_2Cl^+, KCl_2^-, $K_2(OH)^+$, and $K(OH)_2^-$, as well as higher-order polyatomic ion clusters and mixed-ligand complexes, may predominate over single ions and neutral ion pairs in concentrated electrolyte solutions at supercritical temperatures and pressures where the dielectric constant of H_2O is $\leq$ 15 (Oelkers & Helgeson 1990, 1991a, b, 1992a, b).

Acknowledgements

Acknowledgement is made with thanks to the donors of the Petroleum Research Fund, administered by the American Chemical Society, for support of this research (ACS-PRF Grant 23026-AC2). The research also was supported in part by the National Science Foundation (NSF Grant EAR 8606052), the Department of Energy (DOE Grant DE-FG03-85ER-13419), and The Committee on Research at the University of California, Berkeley. We are indebted to Eric Oelkers, Barbara Ransom, and Jan Amend for stimulating discussions and helpful suggestions during the course of this study. Thanks also are due Joan Bossart for word processing, Lillian Mitchell, Rebecca Arington, and Kevin Kwong for drafting figures, Joachim Hampel and Peggy Gennaro for photographic assistance, and Mary Connolly for help in plotting the figures. We are grateful to Yurii Molchanov (Institute of Experimental Mineralogy, USSR Academy of Science) and Yurii Shvarov (Moscow State University) for making available the computer programs PHX and GIBBS, which we used to generate the phase relations discussed above. Finally, we would like to express our gratitude to J.V. Walther, G.M. Anderson, R.F. Martin and an anonymous referee for insightful and helpful reviews of the manuscript.

References

Adams, J.B. (1968): Differential solution of plagioclase in supercritical water. *Am. Mineral.* **53**, 1603-1613.

Adcock, S.W. & Mackenzie, W.S. (1981): The solubility of minerals in supercritical water. *In* Progress in Experimental Petrology, 5th Progress Report of Research Supported by NERC, 9-10.

Althaus, E. & Johannes, W. (1969): Experimental metamorphism of NaCl-bearing aqueous solutions by reaction with silicates. *Am. J. Sci.* **267**, 87-98.

Anderson, G.M. & Burnham, C.W. (1965): The solubility of quartz in supercritical water. *Am. J. Sci.* **263**, 494-511.

_____ & _____ (1967): Reactions of quartz and corundum with aqueous chloride and hydroxide solutions at high temperatures and pressures. *Am. J. Sci.* **265**, 12-27.

_____, Pascal, M.L. & Rao, J. (1987): Aluminum speciation in metamorphic fluids. *In* Chemical Transfer in Metasomatic Processes (H.C. Helgeson, ed.). D. Reidel, Dordrecht, Holland (297-321).

Apps, J.A. & Neil, J.M. (1983): Solubility of albite in the aqueous phase between 125°C and 350°C. *In* Proc. 4th Water-Rock Interaction Symp. (Misasa, Japan), 290-316.

_____, _____ & Jun, C.-H. (1989): Thermodynamic properties of gibbsite, bayerite, boehmite, diaspore, and the aluminate ion between 0 and 350°C. *Lawrence Berkeley Laboratory, Rep.* **21482**.

Baes, C.F., Jr. & Mesmer, R.E. (1976): *The Hydrolysis of Cations*. John Wiley & Sons, New York.

Barnes, I. (1985): Mineral-water reactions in metamorphism and volcanism. *Chem. Geol.* **49**, 21-29.

_____ & O'Neil, J.R. (1969): The relationship between fluids in some fresh alpine-type ultramafics and possible modern serpentinization, western United States. *Geol. Soc. Am. Bull.* **80**, 1947-1960.

Barns, R.L., Laudise, R.A. & Shields, R.M. (1963): The solubility of corundum in basic hydrothermal solvents. *J. Phys. Chem.* **67**, 835-839.

Baumgartner, L.P. & Eugster, H.P. (1988): Experimental determination of corundum solubility and Al-speciation in supercritical H_2O-HCl solutions. *Geol. Soc. Am., Abstr. Programs* **20**, A191.

Becker, K.H., Cemic, L. & Langer, K.E.O.E. (1983): Solubility of corundum in supercritical water. *Geochim. Cosmochim. Acta* **47**, 1573-1578.

Bernshtein, V.A. & Matsenok, Ye.A. (1965): Equilibrium in the reaction of diaspore with solutions of sodium hydroxide at 250° and 300°C. *Zh. Prikl. Khim.* **38**, 1935-1938 (in Russ.).

Bourcier, W.L., Knauss, K.G. & Jackson, K.J.

(1987): Aluminum hydrolysis constants to 250°C determined from boehmite solubility measurements. *Geol. Soc. Am., Abstr. Programs* **19**, 596.

BROWN, G.C. & FYFE, W.S. (1971): Kyanite–andalusite equilibrium. *Contrib. Mineral. Petrol.* **33**, 227-231.

BURNHAM, C.W., RYZHENKO, B.N. & SCHITEL, D. (1973): Water solubility of corundum at 500 – 800°C and 6 kbar. *Geochem. Int.* **8**, 1374.

BUSEY, R.H. & MESMER, R.E. (1977): Ionization equilibria of silicic acid and polysilicate formation in aqueous sodium chloride solutions to 300°C. *Inorg. Chem.* **16**, 2444-2450.

CHANG, B.-T., PAK, L.-H. & LI, Y.-S. (1979): Solubilities and rates of dissolution of diaspore in NaOH aqueous solutions. *Bull. Chem. Soc. Japan* **52**, 1321-1326.

CHEN, C.-T. A. & MARSHALL, W.L. (1982): Amorphous silica solubilities. IV. Behavior in pure water and aqueous sodium chloride, sodium sulfate, magnesium chloride, and magnesium sulfate solutions up to 350°C. *Geochim. Cosmochim. Acta* **46**, 279-287.

COUTURIER, Y., MICHARD, G. & SARAZIN, G. (1984): Constantes de formation des complexes hydroxydes de l'aluminium en solution aqueuse de 20 à 70°C. *Geochim. Cosmochim. Acta* **48**, 649-659.

CRERAR, D.A. & ANDERSON, G.M. (1971): Solubility and solvation reactions of quartz in dilute hydrothermal solutions. *Chem. Geol.* **8**, 107-122.

CURRIE, K.L. (1968): On the solubility of albite in supercritical water in the range 400 to 600°C and 750 to 3500 bars. *Am. J. Sci.* **266**, 225-251.

DAVIS, N.F. (1972): *Experimental Studies in the System Sodium-Alumina Trisilicate-Water. I. The Apparent Solubility of Albite in Supercritical Water. II. The Partial Specific Volume of H_2O in $NaAlSi_3O_8$ Melts with Petrologic Implications.* Ph.D. dissertation, Pennsylvania State Univ., University Park, Pennsylvania.

DE DONDER, T. (1922): L'affinité. Applications aux gaz parfaits. *Acad. Roy. Belgique, Bull. Classe Sci.* 7 (5th Ser.), 197-205.

_____ & VAN RYSSELBERGHE, P. (1936): *Thermodynamic Theory of Affinity: A Book of Principles.* Stanford University Press, Stanford, California.

DRUZHININA, N.K. (1955): Solubility of diaspore in aluminate solutions. *Tsvetnyye Metally* **28**, 54-56 (in Russ.).

ELLIS, A.J. & MAHON, W.A.J. (1964): Natural hydrothermal systems and experimental hot-water/rock interactions. *Geochim. Cosmochim. Acta* **28**, 1323-1357.

FOURNIER, R.O., ROSENBAUER, R.J. & BISCHOFF, J.L. (1982): The solubility of quartz in sodium chloride solution at 350°C and 180 to 500 bars. *Geochim. Cosmochim. Acta* **46**, 1975-1978.

FREDERICKSON, A.F. & COX, J.E., JR. (1954): Mechanism of "solution" of quartz in pure water at elevated temperatures and pressures. *Am. Mineral.* **39**, 886-900.

FRIEDMAN, I.I. (1949): The laboratory growth of quartz. *Am. Mineral.* **34**, 583-588.

FRINK, C.R. & PEECH, M. (1963): Hydrolysis of the aluminum ion in dilute aqueous solutions. *Inorg. Chem.* **2**, 473-474.

FRISCH, C.J. & HELGESON, H.C. (1984): Metasomatic phase relations in dolomites of the Adamello Alps. *Am. J. Sci.* **284**, 121-185.

FYFE, W.S. & MCKAY, D.S. (1962): Hydroxyl ion catalysis of the crystallization of amorphous silica at 330°C and some observations on the hydrolysis of albite solutions. *Am. Mineral.* **47**, 83-89.

GANEEV, I.G. & RUMYANTSEV, V.N. (1974): Solubility of corundum in water at elevated temperatures and pressures. *Geokhimia*, 1402-1403 (in Russ.).

GARRELS, R.M. & MACKENZIE, F.T. (1971): *Evolution of Sedimentary Rocks* . W.W. Norton & Co., Inc., New York.

GUNTER, W.D. & EUGSTER, H.P. (1980): Mica-feldspar equilibria in supercritical alkali chloride solutions. *Contrib. Mineral. Petrol.* **75**, 235-250.

HELGESON, H.C. (1968): Evaluation of irreversible reactions in geochemical processes involving minerals and aqueous solutions. I. Thermodynamic relations. *Geochim. Cosmochim. Acta* **32**, 853-877.

_____ (1970a): A chemical and thermodynamic model of ore deposition in hydrothermal systems. *Mineral. Soc. Am., Spec. Pap.* **3**, 155-186.

_____ (1970b): Description and interpretation of phase relations in geochemical processes involving aqueous solutions. *Am. J. Sci.* **268**, 415-438.

_____ (1979): Mass transfer among minerals and hydrothermal solutions. *In* Geochemistry of Hydrothermal Ore Deposits (H.L. Barnes, ed.). John Wiley & Sons, New York (567-610).

_____ (1987): Application of moderation theorems to metasomatic processes. *In* Chemical Transport in

Metasomatic Processes (H.C. Helgeson, ed.), D. Reidel, Dordrecht, Holland (189-238).

_____, DELANY, J.M., NESBITT, W.H. & BIRD, D.K. (1978): Summary and critique of the thermodynamic properties of rock-forming minerals. *Am. J. Sci.* **278A**.

_____ & KIRKHAM, D.H. (1974): Theoretical prediction of the thermodynamic behavior of aqueous electrolytes at high pressures and temperatures. II. Debye-Hückel parameters for activity coefficients and relative partial molal properties. *Am. J. Sci.* **274**, 1119-1261.

_____ & _____ (1976): Theoretical prediction of the thermodynamic behavior of aqueous electrolytes at high pressures and temperatures. III. Equation of state for aqueous species at infinite dilution. *Am. J. Sci.* **276**, 97-240.

_____, _____ & FLOWERS, G.C. (1981): Theoretical prediction of the thermodynamic behavior of aqueous electrolytes at high pressures and temperatures. IV. Calculation of activity coefficients, osmotic coefficients, and apparent molal and standard and relative partial molal properties to 600°C and 5 kbar. *Am. J. Sci.* **281**, 1249-1516.

_____, MURPHY, W.M. & AAGAARD, P. (1984): Thermodynamic and kinetic constraints on reaction rates among minerals and aqueous solutions. II. Rate constants, effective surface area, and the hydrolysis of feldspar. *Geochim. Cosmochim. Acta* **48**, 2405-2432.

HEMLEY, J.J. (1959): Some mineralogical equilibria in the system K_2O–Al_2O_3–SiO_2–H_2O. *Am. J. Sci.* **257**, 241-270.

_____ & JONES, W.R. (1964): Chemical aspects of hydrothermal alteration with emphasis on hydrogen metasomatism. *Econ. Geol.* **59**, 538-569.

_____, MEYER, C. & RICHTER, D.H. (1961): Some alteration reactions in the system Na_2O–Al_2O_3–SiO_2–H_2O. *U.S. Geol. Surv., Prof. Pap.* **424-D**, 338-340.

_____, MONTOYA, J.W., MARINENKO, J.W. & LUCE, R.W. (1980): Equilibria in the system Al_2O_3–SiO_2–H_2O and some general implications for alteration/mineralization processes. *Econ. Geol.* **75**, 210-228.

HUANG, W.H. & KELLER, W.D. (1972): Standard free energies of formation calculated from dissolution data using specific mineral analyses. *Am. Mineral.* **57**, 1152-1162.

_____ & _____ (1973): Gibbs free energies of formation calculated from dissolution data using specific mineral analysis. III. Clay minerals. *Am. Mineral.* **58**, 1023-1028.

_____ & KIANG, W.C. (1973): Gibbs free energies of formation calculated from dissolution data using specific mineral analysis. II. Plagioclase feldspars. *Am. Mineral.* **58**, 1016-1022.

HÜCKEL, E. (1925): Zur Theorie konzentrierterer wässeriger Lösungen starker Electrolyte. *Phys. Z.* **26**, 93-147.

IVANOV, I.P., BORISOV, M.V. & RED'KIN, A.F. (1979): Thermodynamic and experimental modeling of local equilibria in metasomatic zones of acidic leaching. *In* Problems in Physicochemical Petrology (A.V. Zharikov, ed.). Nauka Press, Moscow (145-176) (in Russ.).

IVANOV, V.V. (1975): Principal geochemical environments and processes of the formation of hydrothermal waters in regions of recent volcanic activity. *In* Geochemistry of Water (Y. Kitano, ed.). Dowden, Hutchinson & Ross, Inc., Stroudsburg, Pennsylvania (328-349).

JÄNECKE, E. (1906): Über eine neue Darstellungsform der wässerigen Lösungen zweier und dreier gleichioniger Salze, reziproker Salzpaare und der van't Hoffschen Untersuchungen über ozeanische Salzablagerungen. *Z. Anorg. Chem.* **51**, 132-157.

JOHNSON, J.W. & NORTON, D. (1991): Critical phenomena in hydrothermal systems: state, thermodynamic, electrostatic, and transport properties of H_2O in the critical region. *Am. J. Sci.* **291**, 541-648.

KENNEDY, G.C. (1950): A portion of the system silica–water. *Econ. Geol.* **45**, 629-653.

KHITAROV, N.I. (1956): The 400° isotherm for the system H_2O–SiO_2 at pressures up to 2,000 kg/cm^2. *Geochem. Int.* **1956**(1), 55-61.

_____ (1957): The chemical properties of solutions arising as a result of the interaction of water with rocks at elevated temperatures and pressures. *Geochem. Int.* **2**(6), 566-578.

KITAHARA, S. (1960a): The solubility of quartz in water at high temperatures and high pressures. *Rev. Phys. Chem. Jpn.* **30**, 109-114.

_____ (1960b): The solubility of quartz in the aqueous sodium chloride solution at high temperatures and high pressures. *Rev. Phys. Chem. Jpn.* **30**, 115-121.

_____ (1960c): The polymerization of silicic acid obtained by the hydrothermal treatment of quartz and the solubility of amorphous silica. *Rev. Phys. Chem. Jpn.* **30**, 131-137.

KITTRICK, J.A. (1966): Free energy of formation of kaolinite from solubility measurements. *Am. Mineral.* **51**, 1457-1466.

_____ (1980): Gibbsite and kaolinite solubilities by immiscible displacement of equilibrium solutions. *Soil Sci. Soc. Am. J.* **44**, 139-142.

KORZHINSKIY, M.A. (1987): Solubility of corundum and possible forms of aluminum in hydrochloric fluids. *Geokhimia* No. 4, 580-585 (in Russ.).

KRETZ, R. (1983): Symbols for rock-forming minerals. *Am. Mineral.* **68**, 277-279.

KUYUNKO, N.S., MALININ, S.D. & KHODAKOVSKIY, I.L. (1983): An experimental study of aluminum hydrolysis at 150, 200, and 250°C. *Geochem. Int.* **20**, 76-86.

LAUDISE, R.A. (1959): Kinetics of hydrothermal quartz crystallization. *J. Am. Chem. Soc.* **81**, 562-566.

_____ & BALLMAN, A.A. (1961): The solubility of quartz under hydrothermal conditions. *J. Phys. Chem.* **61**, 1396-1400.

LEARNED, R.E. (1966): *The Solubilities of Quartz, Quartz-Cinnabar and Cinnabar-Stibnite in Sodium Sulfide Solutions and their Implications for Ore Genesis.* Ph.D. dissertation, Univ. California, Riverside, California.

_____, DICKSON, F.W. & TUNELL, G. (1967): The solubility of quartz in Na_2S and NaOH solutions at elevated temperatures and 100 bars. *Trans. Am. Geophys. Union* **48**, 249 (abstr.).

LEVINSON, S., DOUGLAS, G. & JOHNSON, L.R. (1965): Hydrothermal solubility of Al_2O_3 in $Na_2B_4O_7$ solution. *Am. Mineral.* **50**, 403-410.

LUKASHOV, YU.M., KOMISSAROV, K.B., GOLUBEV, B.P., SMIRNOV, S.N. & SVISTUNOV, E.P. (1975): An experimental investigation of the electrolytic properties of uni-univalent electrolytes at high parameters of state. *Teploenergetika* **22**(12), 78-87.

MACKENZIE, F.T. & GEES, R. (1971): Quartz: synthesis at Earth-surface conditions. *Science* **172**, 533-535.

MAIER, C.G. & KELLEY, K.K. (1932): An equation for the representation of high temperature heat content data. *Am. Chem. Soc. J.* **54**, 3243-3246.

MARSHALL, W.L. & WARAKOMSKI, J.M. (1980): Amorphous silica solubilities. II. Effect of aqueous salt solutions at 25°C. *Geochim. Cosmochim. Acta* **44**, 915-924.

MAY, H.M., HELMKE, P.A. & JACKSON, M.L. (1979): Gibbsite solubility and thermodynamic properties of hydroxy-aluminum ions in aqueous solution at 25°C. *Geochim. Cosmochim. Acta* **43**, 861-868.

_____, KINNIBURGH, D.G., HELMKE, P.A. & JACKSON, M.L. (1986): Aqueous dissolution, solubilities and thermodynamic stabilities of common aluminosilicate clay minerals: kaolinite and smectites. *Geochim. Cosmochim. Acta* **50**, 1667-1677.

MOLCHANOV, YU. I. (1988): An algorithm and computer program to calculate μ_{H^+}(pH)–X phase diagrams. *Abstr. 2nd All-Union Symp. "Thermodynamics in Geology"* (Miass, USSR) **2**, 73-74.

MONTOYA, J.W. & HEMLEY, J.J. (1975): Activity relations and stabilities in alkali feldspar and mica alteration reactions. *Econ. Geol.* **70**, 577-594.

MOREY, G.W. (1957): The solubility of solids in gases. *Econ. Geol.* **52**, 225-251.

_____ & CHEN, W.T. (1955): The action of hot water on some feldspars. *Am. Mineral.* **40**, 996-1000.

_____ & FOURNIER, R.O. (1961): The decomposition of microcline, albite and nepheline in hot water. *Am. Mineral.* **46**, 688-699.

_____, _____ & ROWE, J.J. (1962): The solubility of quartz in water in the temperature interval from 25° to 300°C. *Geochim. Cosmochim. Acta* **26**, 1029-1043.

_____ & HESSELGESSER, J.M. (1951a): The solubility of some minerals in superheated steam at high pressures. *Econ. Geol.* **46**, 821-835.

_____ & _____ (1951b): The solubility of quartz and some other substances in superheated steam at high pressures. *Trans. ASME*, 865-875.

_____ & _____ (1952): The system H_2O–Na_2O–SiO_2 at 400°C. *Am. J. Sci., Bowen Vol.*, 343-371.

MUKHAMET-GALEYEV, A.P., ZOTOV, A.V., POKROVSKII, V.A. & KOTOVA, Z.YU. (1984): Stability of the 1M and $2M_1$ polytypic modifications of muscovite as determined from solubility at 300°C and saturation steam pressure. *Dokl., Earth Science Sect.* **278**, 140-143.

NAGY, K.L. & LASAGA, A.C. (1990): A full rate law for dissolution and precipitation of gibbsite and simultaneous precipitation of gibbsite and kaolinite at 80°C and pH 3. *Geol. Soc. Am., Abstr. Programs* **22**, A159.

NESBITT, H.W. (1978): Graphical representation of material balance and equilibrium relations for minerals sparingly soluble in H_2O. *Contrib. Mineral. Petrol.* **66**, 367-374.

_____ (1984): Equilibrium diagrams displaying

chemical speciation and mineral stabilities in aqueous solutions. *Mineral. Assoc. Can., Short Course Handbook* **10**, 15-44.

NIKOLAEVA, N.M. & TOLPYGINA, L.N. (1969): Hydrolysis of aluminum salts at elevated temperatures. *Izv. Sib. Otd. Akad. Nauk SSSR, ser. Khim. Nauk* (No. 3), 49-55 (in Russ.).

NORDSTROM, D.K., ALPERS, C.N. & BALL, J.W. (1991): Measurement of negative pH values and high metal concentrations in extremely acid mine waters from Iron Mountain, California. *Geol. Soc. Am., Abstr. Programs* **23**, A383.

NOVGORODOV, P.G. (1975): Solubility of quartz in H_2O–CO_2 mixtures at 700°C and pressures of 3 and 5 kbar. *Geochem. Int.* **12**, 122-126.

_____ (1977): On the solubility of quartz in H_2O + CO_2 and H_2O + NaCl at 700°C and 1.5 kb pressure. *Geochem. Int.* **14**, 191-193.

OELKERS, E.H. & HELGESON, H.C. (1988): Calculation of the thermodynamic and transport properties of aqueous species at high pressures and temperatures. Dissociation constants for supercritical alkali metal halides at temperatures from 400° to 800°C and pressures from 500 to 4000 bars. *J. Phys. Chem.* **92**, 1631-1639.

_____ & _____ (1990): Triple-ion anions and polynuclear complexing in supercritical electrolyte solutions. *Geochim. Cosmochim. Acta* **54**, 727-738.

_____ & _____ (1991a): Calculation of the activity coefficients and degrees of formation of neutral ion pairs in supercritical electrolyte solutions. *Geochim. Cosmochim. Acta* **55**, 1235-1251.

_____ & _____ (1991b): Calculation of the dissociation constants and the relative stabilities of polynuclear clusters in supercritical electrolyte solutions. *Geol. Soc. Am., Abstr. Programs* **23**, A213.

_____ & _____ (1992a): Multiple ion association in supercritical aqueous solutions of single electrolytes. *Nature* (in press).

_____ & _____ (1992b): Calculation of dissociation constants and the relative stabilities of polynuclear clusters of 1:1 electrolytes in hydrothermal solutions at supercritical pressures and temperatures. *Geochim. Cosmochim. Acta* (in press).

OSTAPENKO, G.T. & ARAPOVA, M.A. (1971a): Solubility of kyanite, corundum, quartz, and amorphous silica in aqueous HCl solutions at 285°C and 450 bar. *Geokhimia* (No. 7), 781-788 (in Russ.).

_____ & _____ (1971b): Solubility of andalusite and kyanite in water at 420–500°C and 1300 bars and the thermodynamic constants of these minerals. *Geokhimia* (No. 11), 1297-1303 (in Russ.).

_____, KHETCHIKOV, L.N. & BALITSKIY, V.S. (1969): Hydrolysis of aqueous solutions of sodium sulfide and solubility of quartz in these solutions. *Geochem. Int.* **6** (No. 1), 22-28.

_____, RYZHENKO, B.N. & KHITAROV, N.I. (1987): Modeling of dissolution of polymorphic modifications of Al_2SiO_5 in hydrochloric acid solutions at high temperatures and pressures (on the example of kyanite). *Geokhimia* (No. 4), 557-562 (in Russ.).

PASCAL, M.-L. (1984): *Nature et propriétés des espèces en solution dans le système K_2O–Na_2O–SiO_2–Al_2O_3–H_2O–HCl: contribution expérimentale.* Thèse de doctorat, Université Pierre et Marie Curie, Paris, France.

_____ & ANDERSON, G.M. (1989): Speciation of Al, Si, and K in supercritical solutions: experimental study and interpretation. *Geochim. Cosmochim. Acta* **53**, 1843-1855.

_____, PUAYA, V. & ROUX, J. (1989): Corundum solubility in supercritical (K,Na)Cl–H_2O fluids. *3rd Int. Symp. Hydrothermal Reactions (Frunze, USSR), Programs Abstr.*, 50.

PERYEA, F.J. & KITTRICK, J.A. (1988): Relative solubility of corundum, gibbsite, boehmite, and diaspore at standard state conditions. *Clays Clay Miner.* **36**, 391-396.

PETERSEN, U. (1965): Application of saturation (solubility) diagrams to problems in ore deposits. *Econ. Geol.* **60**, 853-893.

PITZER, K.S., PEIPER, J.C. & BUSEY, R.H. (1984): Thermodynamic properties of aqueous sodium chloride solutions. *J. Phys. Chem. Ref. Data* **13**, 1-102.

POKROVSKII, V.A. (1982): Experimental study of the equilibrium 1.5 Ab + 0.5 KCl + HCl = 0.5 Ms + 3 Qu + 1.5 NaCl at 300 to 500°C and 1 kb. *Dokl. Earth Sci. Sect.* **262**, 191-194.

_____ (1989): Theoretical prediction of the differential mobility of components in hydrothermal systems using phase diagrams. *In* Physicochemical Analysis of Mineral Formation Processes (V.A. Zharikov, ed.). Nauka Press, Moscow (212-245) (in Russ.).

_____ & HELGESON, H.C. (1989): New estimates of thermodynamic properties of aqueous aluminum species in the system Al_2O_3–H_2O–NaCl to 5 kb and 1000°C, using the modified Helgeson–Kirkham–

Flowers equation of state. *Geol. Soc. Am., Abstr. Programs* **21**, A156.

_____, _____ & OELKERS, E.H. (1991): A thermodynamic model for mineral-solution equilibria in the system K_2O-Na_2O-Al_2O_3-SiO_2-H_2O-HCl to 700°C and pressures to 5 kb. *Trans. Am. Geophys. Union* **72**(17, Suppl.), 313 (abstr.).

_____ & IVANOV, I.P. (1982): μ_{H^+}-X diagrams for water-mineral systems. *Dokl. Earth Sci. Sect.* **266**, 207-211.

_____ & SOROKIN, V.I. (1983): The solubility phase diagram for the Hg-Sb-S-H_2O system. *Geochem. Int.* **20**(3), 101-117.

POLZER, W.L. & HEM, J.D. (1965): The dissolution of kaolinite. *J. Geophys. Res.* **70**, 6233-6240.

POPP, R.K. & FRANTZ, J.D. (1980): Mineral solution equilibria. III. The system Na_2O-Al_2O_3-SiO_2-H_2O-HCl. *Geochim. Cosmochim. Acta* **44**, 1029-1037.

RAGNARSDÓTTIR, K.V. & WALTHER, J.V. (1983): Pressure sensitive "silica geothermometer" determined from quartz solubility experiments at 250°C. *Geochim. Cosmochim. Acta* **47**, 941-946.

_____ &_____ (1985): Experimental determination of corundum solubilities in pure water between 400-700°C and 1-3 kbar. *Geochim. Cosmochim. Acta* **49**, 2109-2115.

RED'KIN, A.F. & CHEVYCHELOVA, T.K. (1988): Experimental study of solubilities of quartz, diaspore, and kaolinite in presence of diaspore at 300°C, 1 kb, and various ionic strengths. *In* Ocherki Fiziko-khimiheskoi petrologii (V.A. Zharikov, ed.). Nauka Press, Moscow (134-142) (in Russ.).

_____ & _____ (1991): Some mineral equilibria and the composition of coexisting aqueous solutions in the system Al_2O_3-SiO_2-H_2O at 250-430°C and 1 kb. *In* Ocherki fiziko-khimicheskoi petrologii (V.A. Zharikov, ed.). Nauka Press, Moscow (in press).

_____ & IVANOV, I.P. (1980): Experimental study of hydrolytic reactions in the system Al_2O_3-SiO_2-H_2O-HCl. *Dokl. Earth Sci. Sect.* **250**, 209-211.

REESMAN, A.L. & KELLER, W.D. (1965): Calculation of apparent standard free energies of formation of six rock-forming silicate minerals from solubility data. *Am. Mineral.* **50**, 1729-1739.

_____ &_____ (1968): Aqueous solubility studies of high-alumina and clay minerals. *Am. Mineral.* **53**, 929-942.

RICCI, J. E. (1951): *The Phase Rule and Heterogeneous Equilibrium*. D. van Nostrand Co., Inc., New York.

RIMSTIDT, J.D. (1984): Quartz solubility at low temperatures. *Geol. Soc. Am., Abstr. Programs* **16**, 635.

ROOZEBOOM, H.W.B. (1894): Graphische Darstellung der heterogenen Systeme aus ein bis vier Stoffen, mit Einschluss der chemischen Umsetzung. *Z. Phys. Chem.* **15**, 145-158.

SACCOCIA, P.J. & SEYFRIED, W.E., JR. (1990): Talc-quartz equilibria and the stability of magnesium chloride complexes in NaCl-$MgCl_2$ solutions at 300, 350, and 400°C, 500 bars. *Geochim. Cosmochim. Acta* **54**, 3283-3294.

SCHLOEMER, H. (1962): Hydrothermal-synthetische gemeinsame Kristallisation von Orthoklas und Quartz. I. *Radex Rundschau* **3**, 133-157.

SCHOFIELD, R.K. & TAYLOR, A.W. (1954): The hydrolysis of aluminum salt solutions. *J. Chem. Soc.*, 4445-4448.

SCHWARTZENTRUBER, J., FÜRST, W. & RENON, H. (1987): Dissolution of quartz into dilute alkaline solutions at 90°C: a kinetic study. *Geochim. Cosmochim. Acta* **51**, 1867-1874.

SEMENOVA, A.I. & TSIKLIS, D.S. (1970): Solubility of silicon dioxide in water vapor at high pressures and temperatures. *Zh. Fiz. Khim.* **44**, 2505-2508 (in Russ.).

SETCHÉNOW, M. (1892): Action de l'acide carbonique sur les solutions des sels à acides forts. *Ann. Chem. Phys.* **25**, 225-270.

SEWARD, T.M. (1974): Determination of the first ionization constant of silicic acid from quartz solubility in borate buffer solutions to 350°C. *Geochim. Cosmochim. Acta* **38**, 1657-1664.

SHADE, J.W. (1974): Hydrolysis reactions in the SiO_2-excess portion of the system K_2O-Al_2O_3-SiO_2-H_2O in chloride fluids at magmatic conditions. *Econ. Geol.* **69**, 218-228.

SHETTEL, D.L., JR. (1973): Solubility of quartz in H_2O-CO_2 fluids at 5 kb and 500-900°C. *Trans. Am. Geophys. Union* **54**, 480 (abstr.).

_____ (1974): *The solubility of Quartz in Supercritical H_2O-CO_2 Fluids*. M.S. thesis, Pennsylvania State Univ., University Park, Pennsylvania.

SHOCK, E.L. & HELGESON, H.C. (1988): Calculation of the thermodynamic and transport properties of aqueous species at high pressures and temperatures: correlation algorithms for ionic species and equa-

tion of state predictions to 5 kb and 1000°C. *Geochim. Cosmochim. Acta* **52**, 2009-2036.

_____ & _____ (1990): Calculation of the thermodynamic and transport properties of aqueous species at high pressures and temperatures: standard partial molal properties of organic species. *Geochim. Cosmochim. Acta* **54**, 915-945.

_____, _____ & SVERJENSKY, D.A. (1989): Calculation of the thermodynamic and transport properties of aqueous species at high pressures and temperatures: standard partial molal properties of inorganic neutral species. *Geochim. Cosmochim. Acta* **53**, 2157-2183.

_____, OELKERS, E.H., JOHNSON, J.W., SVERJENSKY, D.A. & HELGESON, H.C. (1992): Calculation of the thermodynamic properties of aqueous species at high pressures and temperatures: effective electrostatic radii, dissociation constants, and standard partial molal properties to 1000°C and 5 kb. *J. Chem. Soc. London, Faraday Trans.* (in press).

SHVAROV, YU. V. (1981): *The Algorithms to Determine the Equilibrium Composition of Multicomponent Heterogeneous Systems.* Ph.D. dissertation, Moscow State Univ., Moscow, USSR (author's abstr., 22 p., in Russ.).

SIEVER, R. (1962): Silica solubility, 0°–200°C, and the diagenesis of siliceous sediments. *J. Geol.* **70**, 127-150.

SINITSYN, V.A. (1986): *Hydrothermal Synthesis and Hydrolysis of Minerals from Na-Alkaline Metasomatic Rocks.* Ph.D. dissertation, Institute of Experimental Mineralogy, Moscow, USSR (in Russ.).

_____ & IVANOV, I.P. (1984): Experimental study of the hydrolysis of aegirine in NaOH solutions. *Dokl. Akad. Nauk SSSR* **275**, 1172-1175 (in Russ.).

SOKOLOVA, N.T. & KHODAKOVSKIY, I.L. (1977): The mobility of aluminum in hydrothermal systems. *Geochem. Int.* **14**(3), 105-112.

SOMMERFELD, R.A. (1967): Quartz solution reaction: 400°–500°C, 1000 bars. *J. Geophys. Res.* **72**, 4253-4257.

STRÜBEL, G. (1971): The hydrothermal solubility of muscovite. *Intern. Geochemical Congress, Abstr. Reports (Moscow, USSR)* **I**, 266-267.

SVERJENSKY, D.A., HEMLEY, J.J. & D'ANGELO, W.M. (1991): Thermodynamic assessment of hydrothermal alkali feldspar – mica – aluminosilicate equilibria. *Geochim. Cosmochim. Acta* **55**, 989-1004.

TANGER, J.C., IV & HELGESON, H.C. (1988): Calculation of the thermodynamic and transport properties of aqueous species at high pressure and temperatures: revised equations of state for the standard partial molal properties of ions and electrolytes. *Am. J. Sci.* **288**, 19-98.

TUTTLE, O.F. & FRIEDMAN, I.I. (1948): Liquid immiscibility in the system H_2O–Na_2O–SiO_2. *J. Am. Chem. Soc.* **70**, 919-926.

USDOWSKI, H.E. & BARNES, H.L. (1972): Untersuchungen über das Gleichgewicht zwischen K-Feldspat, Quartz und Muskovit und die Anwendung auf Fragen der Gesteinsbildung bei tieferen Temperaturen. *Contrib. Mineral. Petrol.* **36**, 207-219.

VAN LIER, J.A., DE BRUYN, P.L. & OVERBEEK, J.T.G. (1960): The solubility of quartz. *J. Phys. Chem.* **64**, 1675-1682.

VAN'T HOFF, J.H. (1905): *Zur Bildung der ozenischen Salzablagerungen. I.* Wieweg, Braunschweig.

_____ (1909): *Zur Bildung der ozenischen Salzablagerungen. II.* Wieweg, Braunschweig.

VAREKAMP, J.C. & KREULEN, R. (1990): Exotic fluids: chemistry of the Keli Mutu crater lakes, Flores, Indonesia. *Trans. Am. Geophys. Union* **71**, 1674 (abstr.).

VOLFINGER, M. & ROUX, J. (1991): Determination expérimentale de l'activité de HCl dans les systèmes sodiques. *Bull. Liaison, Soc. franç. Minéral. Cristallogr.* **2**, 54 (abstr.).

VOLOKHOV, Y.A., PAVLOV, L.N., EREMIN, N.I. & MIRONOV, V.E. (1971): Hydrolysis of aluminum salts. *Zh. Prikl. Khim.* **44**, 243-246 (in Russ.).

WALTHER, J.V. & ORVILLE, P.M. (1983): The extraction-quench techniques for determination of the thermodynamic properties of solute complexes: application to quartz solubility in fluid mixtures. *Am. Mineral.* **68**, 731-741.

WEFERS, K.(1967): Zur chemischen Technologie des Bauxitaufschlusses. 1. Das System Na_2O–Al_2O_3–H_2O. *Metall.* **25**, 422-431.

WEILL, D.F. & FYFE, W.S. (1964): The solubility of quartz in H_2O in the range 1000–4000 bars and 400–550°C. *Geochim. Cosmochim. Acta* **28**, 1243-1255.

WENDLANDT, H.G. & GLEMSER, O. (1964): The reactions of oxides with water at high pressures and temperatures. *Angew. Chem., Intern. Ed.* **3**, 47-54.

WINTSCH, R.P., MERINO, E. & BLAKELY, R.F. (1980): Rapid-quench hydrothermal experiments in dilute chloride solutions applied to the muscovite – quartz

– sanidine equilibrium. *Am. Mineral.* **65**, 1002-1011.

WOODLAND, A.B. & WALTHER, J.V. (1987): Experimental determination of the solubility of the assemblage paragonite, albite, and quartz in supercritical H_2O. *Geochim. Cosmochim. Acta* **51**, 365-372.

WRIGHT, J.M., LINDSAY, W.T., JR. & DRUGA, T.R. (1961): The behavior of electrolytic solutions at elevated temperatures as derived from conductance measurements. *Atomic Energy Comm., Res. Devel. Rep.* **WAPD-TM-204.**

WYART, J. & SABATIER, G. (1954): La solubilité des différentes formes de silice dans la vapeur d'eau sous des pressions élevées. *C. R. Acad. Sci., Paris* **238**, 702-705.

_____ & _____ (1955a): Nouvelles mesures de la solubilité du quartz, de la tridymite et de la cristobalite dans l'eau sous pression au-dessus de la température critique. *C. R. Acad. Sci., Paris* **240**, 1905-1907.

_____ & _____ (1955b): Solubilité du quartz dans des solutions de sels alcalins, sous pression au-dessus de la température critique. *C. R. Acad. Sci., Paris* **240**, 2157-2159.

YALMAN, R.G., SHAW, E.R. & CORWIN, J.F. (1960): The effect of pH and fluoride on the formation of aluminum oxides. *J. Phys. Chem.* **64**, 300-303.

YAMAGUCHI, G., YANAGIDA, H. & SOEJIMA, S. (1962): On the solubility and velocity of dissolution of corundum under hydrothermal conditions. *Bull. Chem. Soc. Jpn.* **35**, 1789-1794.

Received April 22, 1991, revised manuscript accepted November 29, 1991.

APPENDIX A. CALCULATION OF THE APPARENT STANDARD PARTIAL MOLAL GIBBS FREE ENERGIES OF FORMATION OF MINERALS AND AQUEOUS SPECIES AT HIGH TEMPERATURES AND PRESSURES

The apparent standard partial molal Gibbs free energy of formation ($\Delta G°$) of a given species at a specified pressure (P) and temperature (T) is defined by

$$\Delta\overline{G}^\circ \equiv \Delta\overline{G}^\circ_f + \left(\overline{G}^\circ_{P,T} - \overline{G}^\circ_{P_r,T_r}\right) \tag{A1}$$

where $\Delta\overline{G}^\circ_f$ refers to the standard partial molal Gibbs free energy of formation of the species from the elements in their stable form at a reference pressure (P_r) and temperature (T_r) of 1 bar and 298.15K, and $\overline{G}^\circ_{P,T} - \overline{G}^\circ_{P_r,T_r}$ stands for the difference in the standard partial molal Gibbs free energy of the species at the pressure and temperature of interest, and that at P_r and T_r. The standard state adopted for minerals and water in the present study is one of unit activity of the thermodynamic components of stoichiometric minerals and pure H_2O at any pressure and temperature. The standard state for aqueous species other than H_2O calls for unit activity of the species in a hypothetical one molal solution referenced to infinite dilution at any pressure and temperature.

The last term on the right side of Eqn. (1) can be expressed for minerals in the crust of the Earth as (Helgeson *et al.* 1978)

$$\begin{aligned}\overline{G}^\circ_{P,T} - \overline{G}^\circ_{P_r,T_r} = &-\overline{S}^\circ_{P_r,T_r}(T-T_r) + a\left(T - T_r - T\ln\left(\frac{T}{T_r}\right)\right) \\ &-\left(\frac{\left(c + bT_r^2T\right)(T-T_r)^2}{2T_r^2T}\right) + \overline{V}^\circ_{P_r,T_r}(P-P_r)\end{aligned} \tag{A2}$$

where *a*, *b* and *c* stand for Maier-Kelley (1932) temperature–pressure-independent coefficients characteristic of the mineral, and $\overline{S}^\circ_{P_r,T_r}$ and $\overline{V}^\circ_{P_r,T_r}$ represent the standard partial molal entropy and volume of the mineral at 25°C and 1 bar, respectively.

The parenthetical term in Eqn. (A1) for charged aqueous species can be written as (Tanger & Helgeson 1988)

$$\begin{aligned}\overline{G}^\circ_{P,T} - \overline{G}^\circ_{P_r,T_r} = &-\overline{S}^\circ_{P_r,T_r}(T-T_r) - c_1\left(T\ln\left(\frac{T}{T_r}\right) - T + T_r\right) \\ &+ a_1(P-P_r) + a_2\ln\left(\frac{\Psi+P}{\Psi+P_r}\right) \\ &- c_2\left(\left(\left(\frac{1}{T-\Theta}\right) - \left(\frac{1}{T_r-\Theta}\right)\right)\left(\frac{\Theta-T}{\Theta}\right) - \frac{T}{\Theta^2}\ln\left(\frac{T_r(T-\Theta)}{T(T_r-\Theta)}\right)\right) \\ &+ \left(\frac{1}{T-\Theta}\right)\left(a_3(P-P_r) + a_4\ln\left(\frac{\Psi+P}{\Psi+P_r}\right)\right) \\ &+ \omega\left(\frac{1}{\varepsilon} - 1\right) - \omega_{P_r,T_r}\left(\frac{1}{\varepsilon_{P_r,T_r}} - 1\right) + \omega_{P_r,T_r}Y_{P_r,T_r}(T-T_r),\end{aligned} \tag{A3}$$

where a_1, a_2, a_3, a_4, c_1, and c_2 represent temperature–pressure-independent coefficients characteristic of the species, Θ and Ψ stand for solvent parameters equal to 228 K and 2600 bars, respectively, ϵ refers to the dielectric constant of H_2O, Y_{P_r,T_r} denotes a constant equal to –5.80 $\times 10^{-5}$ K^{-1}, $\overline{S}^\circ_{P_r,T_r}$ designates the standard partial molal entropy of the species at 25°C and 1 bar, and ω designates the conventional Born coefficient of the species, which can be expressed for the *j*th such species as

$$\omega_j = \eta\left(Z_j^2\left(r_{e,j,P_r,T_r} + |Z_j|g\right)^{-1} - Z_j(3.082+g)^{-1}\right) \tag{A4}$$

where r_{e,j,P_r,T_r} refers to the effective electrostatic radius of the species at the reference pressure and temperature, which for monatomic ions is given by (Helgeson & Kirkham 1976)

$$r_{e,j,P_r,T_r} = r_{x,j} + |Z_j|kz \tag{A5}$$

and for other charged aqueous species by (Shock & Helgeson 1988)

$$r_{e,j,P_r,T_r} = \frac{Z_j^2\left(\eta Y_{P_r,T_r} - 100\right)}{\overline{S}^\circ_{j,P_r,T_r} - \alpha_Z} \tag{A6}$$

where Z_j represents the charge on the *j*th aqueous species, r_{xj} refers to the crystallographic radius of the species, $\eta = 1.66027 \times 10^5$ Å cal mol^{-1}, *kz* designates a constant equal to 0.94 Å for cations and 0.0 A for anions, *g* stands for a solvent function of temperature and density given by Shock *et al.* (1992), $\overline{S}^\circ_{j,P_r,T_r}$ denotes the standard partial molal entropy of the *j*th aqueous species at the reference pressure (P_r) and temperature (T_r), and α_Z is defined by

$$\alpha_Z \equiv 71.5|Z_j| \tag{A7}$$

The analog of Eqn. (A3) for neutral aqueous species can be written as (Shock *et al.* 1989, Shock & Helgeson 1990)

$$\begin{aligned}\overline{G}^\circ_{P,T} - \overline{G}^\circ_{P_r,T_r} = &-\overline{S}^\circ_{P_r,T_r}(T-T_r) - c_1\left(T\ln\left(\frac{T}{T_r}\right) - T + T_r\right) \\ &+ a_1(P-P_r) + a_2\ln\left(\frac{\Psi+P}{\Psi+P_r}\right) \\ &- c_2\left(\left(\left(\frac{1}{T-\Theta}\right) - \left(\frac{1}{T_r-\Theta}\right)\right)\left(\frac{\Theta-T}{\Theta}\right) - \frac{T}{\Theta^2}\ln\left(\frac{T_r(T-\Theta)}{T(T_r-\Theta)}\right)\right) \\ &+ \left(\frac{1}{T-\Theta}\right)\left(a_3(P-P_r) + a_4\ln\left(\frac{\Psi+P}{\Psi+P_r}\right)\right) \\ &+ \omega_e\left(Y_{P_r,T_r}(T-T_r) + \frac{1}{\varepsilon_{P,T}} - \frac{1}{\varepsilon_{P_r,T_r}}\right),\end{aligned} \tag{A8}$$

where ω_e denotes the effective Born coefficient of the species, which is independent of pressure and temperature and consistent with

$$\omega_e = \hat{a} + \hat{b}\,\overline{S}^\circ_{P_r,T_r} \tag{A9}$$

where $\hat{a}$ and $\hat{b}$ stand for correlation parameters for various groups of neutral aqueous species given by Shock *et al.* (1989) and Shock & Helgeson (1990).

Equations (A1) – (A9) permit calculation of the apparent standard partial molal Gibbs free energies of formation of minerals and aqueous species at elevated temperatures and pressures, which can be used to calculate equilibrium constants for reactions among them from

$$\log K = -\frac{\Delta\overline{G}^\circ_r}{2.303RT} \tag{A10}$$

where

$$\Delta\overline{G}^\circ_r = \sum_i \hat{n}_{i,r}\Delta\overline{G}^\circ_i \tag{A11}$$

where $\Delta\bar{G}°_l$ stands for the apparent standard partial molal Gibbs free energy of formation of the lth species in the reaction given by an appropriate statement of Eqn. (A1), and $\hat{n}_{l,r}$ denotes the reaction coefficient for the species in the rth reaction, which is positive for products and negative for reactants.

Appendix B. Calculation of Activity Coefficients of Aqueous Species at High Temperatures and Pressures

Close approximation of the activity coefficients of charged aqueous species (designated by the subscript j) in aqueous solutions in which the electrolyte MX predominates over other solutes by an order of magnitude or more can be calculated over a wide range of concentration from the Hückel (1925) equation, which can be expressed as (Helgeson *et al.* 1981)

$$\log\bar{\gamma}_j = -\frac{A_\gamma Z_j^2 \bar{I}^{1/2}}{1+\mathring{a}_{MX} B_\gamma \bar{I}^{1/2}} + \Gamma_\gamma + b_{\gamma,MX}\bar{I} \qquad \text{(B1)}$$

where A_γ and B_γ stand for Debye-Hückel solvent parameters, $\mathring{a}_{MX}$ and $b_{\gamma,MX}$ denote the ion size and extended term parameters for the subscripted electrolyte, Z_j stands for the charge on the jth species, Γ_γ designates the conversion factor of mole fraction to molality, given by $\Gamma_\gamma = -\log(1 + 0.0180153\ m^*)$, where m^* refers to the sum of molalities of all of the solute species, and $\bar{I}$ stands for the effective ionic strength of the solution on the molal scale of concentration, which is given by

$$\bar{I} = \frac{1}{2}\sum_j Z_j^2 m_j \qquad \text{(B2)}$$

where m_j represents the molality of the jth species. The values of A_γ and B_γ for H_2O, and $\mathring{a}_{MX}$ and $b_{\gamma,MX}$ for NaCl used in the present study were computed as functions of temperature and pressure using equations and parameters taken from Helgeson & Kirkham (1974), Shock *et al.* (1992), and Oelkers & Helgeson (1990), respectively.

The activity coefficients for neutral aqueous species in the electrolyte solution discussed above can be calculated at high temperatures and pressures from the Setchénow (1892) equation (Oelkers & Helgeson 1991a), which can be expressed for the molality scale of concentration as (Helgeson *et al.* 1981)

$$\log\bar{\gamma}_n = b_{\gamma,n,MX}\bar{I} + \Gamma_\gamma \qquad \text{(B3)}$$

where $b_{\gamma,n,MX}$ stands for the Setchénow coefficient for the nth neutral aqueous species in an electrolyte solution in which the electrolyte represented by MX predominates over other solute species by an order of magnitude or more. The Setchénow coefficients for NaCl° and KCl° used in the solubility calculations described in the text were generated by Helgeson *et al.* (1981) and Pokrovskii *et al.* (1991) from osmotic and stoichiometric mean activity coefficients reported in the literature. Computed values of the Setchénow coefficients for NaCl° and KCl° in NaCl and KCl solutions, respectively, are shown in Figure B1 for temperatures from 0° to 350°C at P_{SAT}. It

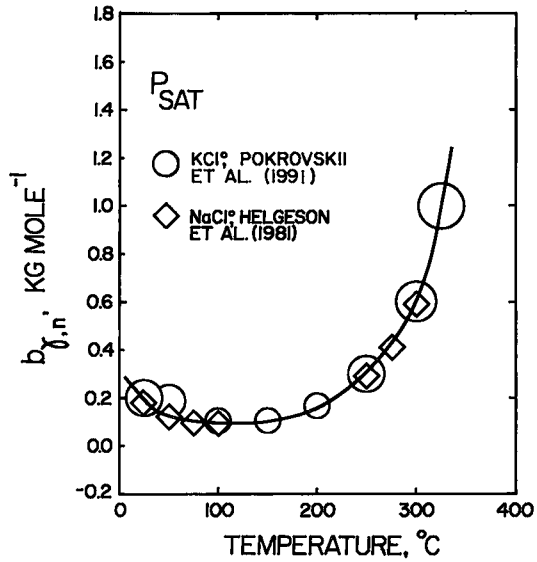

FIG. B1. Setchénow coefficients for KCl° in KCl solutions and NaCl° in NaCl solutions as a function of temperature at P_{SAT} (see text). The curve represents a smooth interpolation of the experimental values of $b_{\gamma,n}$ represented by the symbols.

can be seen in this figure that $b_{\gamma,n}$ for both species decreases with increasing temperature from 0° to ~125°C, where it minimizes. With further increase in temperature, $b_{\gamma,n}$ in Figure B1 increases to an increasing degree. Note in Figure B1 that the Setchénow coefficients for KCl° in KCl solutions and NaCl° in NaCl solutions are nearly identical. It thus appears that in a first approximation, $b_{\gamma,n,MX°}$ can be taken to be the same in KCl and NaCl solutions. Accordingly, the activity coefficients of HCl°, NaOH°, KOH°, $NaAl(OH)_4$°, $KAl(OH)_4$°, NaH_3SiO_4°, and KH_3SiO_4° in NaCl solutions were assumed in the present study to be equal to those of NaCl° in NaCl solutions shown in Figure B1.

The Setchénow coefficients for aqueous silica used in the solubility calculations described in the text were calculated by V.A. Pokrovskii & H.C. Helgeson (in prep.) from experimental solubilities of amorphous silica in aqueous solutions of NaCl reported by Marshall & Warakomski (1980) and Chen & Marshall (1982). This was done by first computing values of the difference function represented by

$$\rho^*_{\bar{\gamma}_n} \equiv \log\bar{\gamma}_n - \Gamma_\gamma \qquad \text{(B4)}$$

Values of $\rho^*_{\bar{\gamma}_n}$ computed from Eqn. (B4) using values of $\bar{\gamma}_n$ retrieved from experimental data can be plotted as a function of $\bar{I}$ to generate values of $b_{\gamma,n}$ from

$$\rho^*_{\bar{\gamma}_n} = b_{\gamma,n}\bar{I} \qquad \text{(B5)}$$

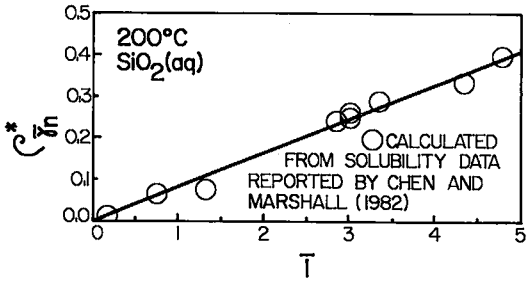

FIG. B2. Plot of Eqn. (B5) for SiO_2° in NaCl solutions at 200°C and P_{SAT} (see text).

An example of such a plot is shown in Figure B2, where value of $\rho^*_{\gamma n}$ computed from the experimental solubilities of amorphous silica in NaCl solutions at 200°C and P_{SAT} reported by Chen & Marshall (1982) are plotted against the effective ionic strength, which was computed using the logarithm of the dissociation constant for NaCl° at 200°C and P_{SAT} given by Shock *et al.* (1992). It can be seen in Figure B2 that all but one of the experimental value of $\rho^*_{\gamma n}$ fall on a straight line consistent with Eqn. (B5). Owing to the paucity of experimental data on solubility of aluminum hydroxides in aqueous alkali metal chloride solutions, the Setchénow coefficient for $Al(OH)_3^\circ$ was assumed in the present study to be equal to that of SiO_2°, which introduces negligible uncertainty in the calculations (Pokrovskii & Helgeson 1989).